Soil Biology and Biochemistry 210 (2025) 109953

Contents lists available at ScienceDirect

Soil Biology and Biochemistry

journal homepage: www.elsevier.com/locate/soilbio

A long road to soil health restoration: earthworms and soil structure show partial recovery in 18-year-old forest skid trails

Maximilian Behringer [a,b,*], John Koestel [c], Bart Muys [d], Karin Wriessnig [a,e], Markus Bieringer [a], Matthias Schlögl [b], Klaus Katzensteiner [a]

[a] BOKU University, Institute of Forest Ecology, Department of Ecosystem Management, Climate and Biodiversity, Vienna, Austria
[b] BOKU University, Institute of Mountain Risk Engineering, Department of Landscape, Water and Infrastructure, Vienna, Austria
[c] Agroscope, Soil and Environment, Zürich, Switzerland
[d] KU Leuven, Department of Earth and Environmental Sciences, Leuven, Belgium
[e] BOKU University, Institute of Applied Geology, Department of Landscape, Water and Infrastructure, Vienna, Austria

ARTICLE INFO

Keywords:
Soil health
Timber harvesting
Forestry
Skid trail
Earthworms
X-ray tomography
Vienna woods

ABSTRACT

Compaction may impair soil health for decades. In a controlled experiment on clayey temperate forest soils, we assessed the effects of ground-based timber harvesting on earthworm abundance and soil structure. We compared freshly trafficked skid trails with those created 18 years ago at the same site. Earthworms were sampled in the ruts of the skid trails and in adjacent undisturbed plots. In addition, we collected undisturbed soil cores at 5 and 15 cm depths for X-ray imaging to assess soil structure.

We identified five earthworm species: *Aporrectodea rosea*, *Dendrobaena depressa*, *Dendrodrilus rubidus*, *Lumbricus rubellus*, and *Octolasion lacteum*. Earthworm abundance was highest on 18-year-old skid trails, particularly of endogeic and juvenile anecic individuals. The abundance of adult anecics remained reduced.

The X-ray data showed that imaged porosity declined sharply after trafficking (from 14.4 ± 5.0 % to 3.5 ± 1.6 % at 5 cm; and from 13.5 ± 4.9 % to 2.0 ± 1.1 % at 15 cm) but recovered at 5 cm within 18 years (12.2 ± 4.3 %), with only partial recovery at 15 cm (7.1 ± 2.5 %). Other structural parameters including biopores, pore anisotropy and Γ-connectivity (connectivity probability; dimensionless local connectivity measure, confined to the range [0,1]) and bulk density followed similar trends. However, the anisotropy of rock fragments did not recover. Pressure and shear forces during harvesting aligned the rock fragments horizontally.

Our data show that earthworms can recolonize compacted forest soils, but recovery of soil structure is depth-dependent and remains incomplete at 15 cm depth after 18 years, resulting in a highly biological active layer sitting on top of a hard pan.

1. Introduction

Soil compaction adversely affects soil health (Nazari et al., 2021; Shah et al., 2017; Shestak and Busse, 2005). It strongly alters soil structure (Bottinelli et al., 2014b; Hansson et al., 2018) and affects soil organisms (Beylich et al., 2010). In forestry timber harvesting is a major cause of soil compaction. Although timber harvesting is infrequent in Central Europe due to long rotation periods, the consequences of soil compaction can persist for decades (DeArmond et al., 2021; Ebeling et al., 2016). This issue has been exacerbated by the increasing use of heavy timber harvesting machinery in recent decades (Cambi et al., 2015), with weights of up to 70 t (Riggert et al., 2019). The greatest compaction of forest soils, which generally have a well-structured topsoil (Klöffel et al., 2022) that is rich in macropores (Hansson et al., 2018; Jost et al., 2012), occurs during the first passage (Cambi et al., 2015). However, subsequent trafficking further amplifies the impact on soil (Grünberg et al., 2025). Several reviews summarize the effects of timber harvesting on soil properties and their recovery (e.g., Cambi et al., 2015; DeArmond et al., 2021; Nazari et al., 2023; Picchio et al., 2020).

Biological parameters have received less attention in recovery studies (DeArmond et al., 2021), despite the fact that soil invertebrates strongly affect ecosystem functions (Wu et al., 2025) and may be a key driver of forest soil restoration (Ampoorter et al., 2011). Macrofaunal

* Corresponding author. BOKU University, Institute of Forest Ecology, Department of Ecosystem Management, Climate and Biodiversity, Vienna, Austria.
E-mail address: maximilian.behringer@boku.ac.at (M. Behringer).

https://doi.org/10.1016/j.soilbio.2025.109953
Received 12 June 2025; Received in revised form 18 August 2025; Accepted 20 August 2025
Available online 20 August 2025

activity, e.g., earthworms and root growth can create new macropores (Jačka et al., 2021; Koestel and Schlüter, 2019) and support the recovery of soil structure (Bottinelli et al., 2014b; Ducasse et al., 2021). Some earthworm species were shown to burrow in highly compacted forest soils (i.e., bulk densities greater than 1.4 g cm^{-3}) (Ampoorter et al., 2011; Ducasse et al., 2021). However, compaction reduces the burrowing rate of earthworms (Arrázola-Vásquez et al., 2022). X-ray imaging from mesocosm experiments has shown that increasing bulk density markedly reduces the length, volume, and continuity of endogeic earthworm burrows (i.e., mostly horizontal burrows created by soil-dwelling earthworm species) (Capowiez et al., 2021). Similar results were observed for *Lumbricus terrestris* in repacked forest soil columns (Ducasse et al., 2021).

Shortly after timber harvesting, earthworm populations in skid trails are drastically reduced across all groups (Bottinelli et al., 2014a; Sohrabi et al., 2020b). Bottinelli et al. (2014a) found that the rut habitats remained unsuitable for earthworms even after 4 years, while Ampoorter et al. (2011) reported increased endogeic earthworm abundance in ruts 3 years after harvesting. Sohrabi et al. (2022, 2020) documented a steady, though incomplete, recovery over 20–25 years. These contrasting findings suggest that the impact of timber harvesting on earthworms – and their subsequent recovery – is highly context dependent. Tree species composition and the related litter nutrient concentrations, for example, have been shown to shape earthworm communities (Desie et al., 2020; Schelfhout et al., 2017).

Similarly, comprehensive studies on forest soil structure using imaging techniques remain scarce. Despite their potential to provide significant insights into soil functions (Rabot et al., 2018), advanced methods like X-ray imaging remain underutilized. Hansson et al. (2018) assessed the immediate effect of timber harvesting in boreal forests on soil structure on a sandy loam using X-ray imaging. They showed a reduction in image-resolved pores (−12 – 24 % in 0–5 cm) and lower connectivity after the harvesting. Structural changes after timber harvesting and short-term recovery (2–3 years) on a silty loam were investigated by Bottinelli et al. (2014b) using 2D-images of thin polished sections. Their results showed a strong reduction in macroporosity (−93 % in 0–7 cm) and a slow recovery of large macropores. Image-derived soil structure has been studied more frequently in compacted agricultural soils (e.g., Mossadeghi-Björklund et al., 2016; Pöhlitz et al., 2019), showing a reduction in mean macropore diameters, isotropy, macropore volume, connectivity and changes in pore size distribution (Pöhlitz et al., 2019). Coinciding with the reduced isotropy remaining macropores show a horizontal orientation (Bottinelli et al., 2014b).

The overall recovery of forest soils in skid trails is a slow process over several decades, with slower recovery of fine-textured soils (DeArmond et al., 2021). This may be due to limited aeration in skid trails (Hansson et al., 2019), which could be more pronounced in clayey soils (Behringer et al., 2025) and delay biological recovery processes.

First effects of soil structure recovery were observed in loamy temperate forest soils 15–25 years after wheeling (Von Wilpert and Schäffer, 2006). Recovery of soil structure follows a depth gradient (Bottinelli et al., 2014b), which has also been observed for other soil parameters (DeArmond et al., 2023; Flores Fernández et al., 2019; Page-Dumroese et al., 2006; Schäffer, 2022). Upper soil layers recover more quickly due to greater fluctuations in temperature and moisture (freezing, swelling and shrinking) as well as higher root growth (Bottinelli et al., 2014b) and biological activity (Bellabarba et al., 2024; Naylor et al., 2022). However, despite the recovery of the upper topsoil, the compacted layers below continue to influence the soil conditions above (DeArmond et al., 2023). Detailed insights into the recovery of soil structure and earthworms, especially over more than a decade, are largely lacking.

In our study we hypothesize that (I) timber harvesting has an immediate and significant impact on soil structure and earthworm populations; (II) earthworms recolonize highly compacted forest soils and thereby support the recovery of soil structure (III); there is recovery of earthworm populations after 18 years; and (IV) structural recovery follows a depth gradient with less recovery at greater depth.

To test our hypotheses, we applied X-ray imaging on undisturbed soil cores sampled from recently trafficked (<1 year) and old skid trails (18 years) and adjacent untrafficked forest soil as control along with physical and chemical soil analyses and earthworm sampling.

2. Material and methods

2.1. Study site and experimental design

The experimental field site, Steinplattl (48°07′24.93“N 16°02′51.68“E, 530 AMSL), is located on a south facing slope in the Flysch zone of the Vienna Woods. The site is dominated by European beech (*Fagus sylvatica* L.) with an admixture of sessile oak (*Quercus petraea* (Matt.) Liebl.), European larch (*Larix decidua* Mill.), sycamore maple (*Acer pseudoplatanus* L.), wild cherry (*Prunus avium* L.) and Norway spruce (*Picea abies* (L.) H. Karst.). Before timber harvesting the mean DBH (diameter at breast height) was 38 cm and the basal area 40 m^2 ha^{-1}. The soil type is a Stagnic Cambisol (IUSS Working Group, 2022) with mull humus dynamic (Zanella et al., 2019). Example soil profiles of the site can be found in the appendix of Behringer et al. (2025). The overall soil mineralogical composition (n = 3) is dominated by quartz (54.3 ± 2.1 %), followed by muscovite (23.3 ± 3.3 %), chlorite (10.7 ± 1.7 %), plagioclase feldspar (albite) (5.3 ± 2.4 %), kaolinite (5.7 ± 1.7 %), and goethite (0.7 ± 0.5 %).

Selective timber harvesting on defined skid trails was performed in the winter of 2004/05 and 2022/23. The use of a new skid trail network in 2022/23 allows us to assess the recovery of the old skid trails. In 2004/05, a total of 440 m^3 of timber was harvested from the 19 ha study site using a skid trail network with a cumulative length of 2900 m. This corresponds to a harvesting intensity of approximately 0.15 m^3 of timber per meter of skid trail. The timber harvesting operation was carried out with a Skogsjan 487 harvester (14 t; 4 wheels) (Skogsjan, Söderhamn, Sweeden) and forwarders by Skogsjan (1088 XL) and EcoLog (564B) (EcoLog, Söderhamn, Sweeden) each with two bogie axles (8 wheels, ca. 12 t + 12 t load). No bogie tracks were used. In 2022/23 741 m^3 timber were harvested on the six harvester/forwarder skid trails (2080 m), resulting in a harvesting-intensity of ca. 0.36 m^3m^{-1}. A John Deere 1270G harvester (22.9 t) and 1210G forwarder (16.2 t + 13 t load) (John Deere, Moline, IL, USA) were used in 2022/23. Both machines were assisted by the ecoforst T-Winch 10.1 (ecofrost GmbH, Groβlobming, Austria) to improve traction. In 2022/23 the analyzed skid trails were logged mostly without bogie tracks (due to wet conditions the forwarder had to use bogie tracks on one axis on all skid trails to improve traction). Further details on the site and the timber harvesting operations 2022/23 can be found in Behringer et al. (2025).

The sampling plots were all located on the 19 ha field site *Steinplattl* at mid slope position with an inclination of ca. 20 % (Supplement 1, Fig. S1). We investigated two treatment pairs: skid trails sampled less than 1 year after harvesting (H01) with their corresponding untrafficked reference plots (C01), and skid trails sampled 18 years after harvesting (H18) with their respective references (C18). Three different skid trails with a spacing of ≥40 m were sampled per treatment. For earthworm sampling, three replicate plots were established within each skid trail, spaced at least 20 m apart (details in 2.2 Earthworm sampling and analyses). One soil profile pit and one adjacent untrafficked pit as control were excavated per skid trail and sampled for X-ray imaging (details in 2.3 Soil sampling and analyses). We extracted three undisturbed soil cores per depth from each pit (Fig. 1). Site conditions (soil volumetric water content, soil temperature and precipitation) during the sampling campaign can be found in Supplement 1, Fig. S2.

2.2. Earthworm sampling and analyses

Earthworms were sampled in April 2023 in plot pairs of trafficked

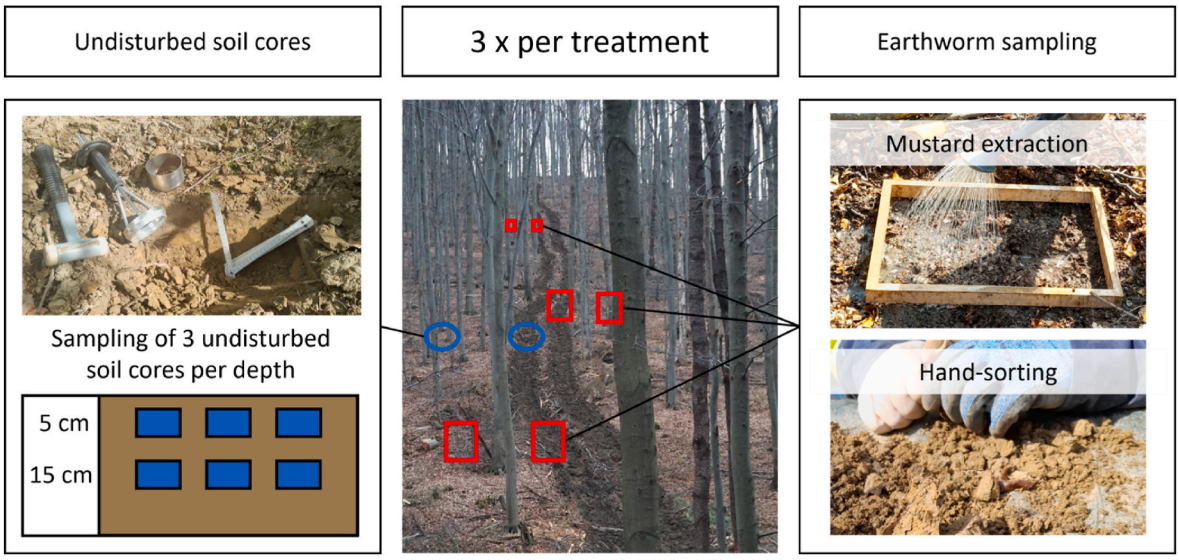

Fig. 1. Experimental design; markers in the ruts show compacted treatments (H01/H18) and markers next to the ruts the controls (C01/C18).

and untrafficked sections (2–5 m distance from the skid trail). Three skid trails with three pairs each were sampled (Fig. 1). Pairs were at least 20 m apart, hence non-autocorrelated independent samples between pairs can be expected (Valckx et al., 2011). For our sampling we used a combined method following Schelfhout et al. (2017) and Valckx et al. (2011) with a few small adaptions. In short, first the litter layer was removed and searched for litter dwelling earthworms within a 0.25 m^2 (61 × 41 cm) frame. Then two applications of mustard solution, with 10 l water and a mustard concentration of 3 g l^{-1} for the first, and 6 g l^{-1} for the second application were sprinkled on the plot. Emerging earthworms were collected for 15 min after each application. Finally, in the center of the plot a soil column of 30 × 30 cm (0.09 m^2) with a depth of 20 cm was dug out for hand sorting. All earthworms were stored in 95 % ethanol and further processed as described in Schelfhout et al. (2017). We assessed earthworm abundance and biomass. All earthworms were weighed individually after ethanol preservation, including gut contents. In a first step adult earthworms were identified using different keys (Christian and Zicsi, 1999; Schaefer, 1992; Sims and Gerard, 1985). If necessary, names were adjusted according to the Drilobase database (http://taxo.drilobase.org). Due to the distinct morphological characteristics of the species found, we could in a second step identify juvenile individuals. Fragments with large missing parts were excluded from further analysis.

All species were assigned to functional groups according to Capowiez et al. (2024). Functional groups for species not covered in Capowiez et al. (2024) were assigned following their suggestions based on the revisited ecological categories of Bouché (1972) by Bottinelli et al. (2020). This applies to *Dendrobaena depressa* (Rosa, 1893) (*Dendrobaena platyura depressa* in Bottinelli et al. (2020)) and *Dendrodrilus rubidus* (Savigny, 1826). The following groups were assigned: litter dweller (*Dendrodrilus rubidus*, *Lumbricus rubellus* (Hoffmeister, 1843)), intermediate (*Aporrectodea rosea* (Savigny, 1826), *Octolasion lacteum* (Orley, 1885)), and burrower (*Dendrobaena depressa*). The two intermediate species were originally assigned as endogeic species (Bouché, 1972) and have the highest functional percentages in the endogeic group as well (Capowiez et al., 2024).

2.3. Soil sampling and analyses

Undisturbed soil cores (aluminum, 250 cm^3, 5 cm height) were cautiously collected in June 2023 at two depth intervals: 5 cm (2.5–7.5 cm) and 15 cm (12.5–17.5 cm) using a hammer with nylon caps and impact absorbing design (Fig. 1, left). Due to high rock fragment content, deeper sampling was not feasible. In total 72 soil cores were collected (two treatment-control pairs (H01 & C01 and H18 & C18), hence 4 × 3 skid trails (blocks) × 2 depth levels × 3 point replicates in every soil sampling pit. During sampling soil moisture was well below field capacity. The cores were carefully transported to the laboratory and stored at 4 °C between processing steps. First, all soil cores were scanned using X-ray imaging (see next section). Fine earth bulk density and total carbon and nitrogen content were determined for all cores.

Fine earth (<2 mm) bulk density was determined by dividing the weight of oven dry (at 105 °C to constant weight) fine earth through its volume as described in Grünberg et al. (2025). The density of rock fragments for volume correction was adjusted to 2.68 ± 0.02 g cm^{-3} which was measured by pycnometry (AccuPyc 1330, micromeritics, Norcross, GA, USA) on 14 composite samples.

Total carbon and nitrogen content were measured on homogenized samples using the elemental analyzer LECO TruSpec (LECO, St. Joseph, MI, USA).

Soil texture and clay mineralogy were analyzed on one soil core per point repetition. To disperse the samples and destroy organic matter, 10 % hydrogen peroxide and an ultrasonic treatment were used. Soil texture was determined from a dry subsample >10 g by wet sieving (630 μm, 200 μm, 63 μm, 20 μm) and for particles <20 μm, sedimentation analysis (SediGraph III, micromeritics, Norcross, GA, USA).

Clay mineral sample preparation followed the methods described by Whittig (1965) and Tributh (1991). The clay fraction (≤2 μm) was separated from the <20 μm sieved sample by centrifugation (5 min at 1000 rpm) and treated with 4 N $MgCl_2$ or 4 N KCl to saturate the sorption complex with magnesium or potassium. 20 mg of clay were placed on porous ceramic plates (Kinter and Diamond, 1956), dried overnight over saturated NH_4NO_3, and then analyzed by X-ray diffraction (Panalytical X'Pert Pro MPD diffractometer, Malvern Panalytical, Malvern, United Kingdom) with an automatic divergence slit, Cu LFF tube (45 kV, 40 mA), and an X'Celerator detector. The measurement time was 25 s, with a step size of 0.017° from 2° to 70° 2θ. To identify swelling clay minerals (smectite, vermiculite), the plates were exposed to an ethylene glycol atmosphere. Potassium-saturated plates were also treated with dimethyl sulfoxide to identify well-crystallized kaolinite. To detect primary chlorite, the plates were heated at 300 °C and 550 °C for 2 h each. X-ray diffraction was performed after each treatment, using specific 2θ ranges based on the treatment type. The clay mineral identification followed Brindley and Brown (1982), Moore and Reynolds (1989), Thorez (1975) and Wilson (1987). The remaining untreated clay fraction was freeze-dried, homogenized, prepared as a powder, and analyzed

analogously. Due to the occurring mixed layers, the peak areas were ranked based on relative shares of the respective clay mineral.

Due to the similarities in clay mineralogy and texture between all samples, the overall soil mineralogical composition was only evaluated from three randomly selected samples. The qualitative mineral composition was determined from these measurements using the Rietveld refinement in the Panalytical HighScore software (Malvern Panalytical, Malvern, United Kingdom).

Soil pH in H_2O was measured according to Austrian Standards L 1083 (Austrian Standards, 2006) on soil samples (0–20 cm) taken during earthworm sampling. The soil-to-water ratio used for the analysis was 1:5 (volumetric).

2.4. X-ray image analysis

Direct assessment of soil structure using imaging techniques provides a more complete understanding of compaction effects (Pöhlitz et al., 2019) than frequently used indirect methods, such as penetration resistance or bulk density. Imaging techniques offer insights into pore connectivity and orientation. They also yield an estimation for the fraction of biopores as well as for soil aeration. To obtain X-ray images we used a GE vtomex s 240 X-ray scanner (with a GE DXR250 HCD (4 MP) detector plate with 2024 × 2024 crystals in x and y directions) (GE Sensing Inspection Technologies GmbH, Wunstorf, Germany) located at the Institute of Crop Science at the ETH Zürich. The scans were taken at a voltage of 170 kV with an electron flow corresponding to 500 μA. Exposure time per radiograph was 200 μs and 2098 radiographs were taken for each core in 2 × 2 binning mode. A 0.7 mm Cu filter was used to decrease beam-hardening artifacts. Image reconstruction was performed with GE software datos 2.1. The final 3D 16-bit TIFF-stacks had a voxel size of 100 μm in all directions.

In the next steps we used the ImageJ (Schindelin et al., 2012) plugin SoilJ (Koestel, 2018) to straighten and center the cores, detect the column walls and to calibrate grey values of the images (column wall grey value = 20000; grey value air inside core = 5000; Fig. 2, a and d). The calibrated greyscale images were segmented into material classes using the pixel classification workflow in *ilastik*, a supervised machine-learning based approach that employs a random forest classifier with 100 trees (Berg et al., 2019). In our classification approach we followed the methods published in Leuther et al. (2023) and Schlüter et al. (2022). The four trained material class labels were pores, organic materials, soil matrix and rock fragments (Fig. 2b and c and e). The classifier was trained on various features including the grey value, edges and texture with different levels of Gaussian smoothing (σ = [0.3, 0.7, 1.0, 1.6, 3.5, 5.0, 10]). One classifier (out-of-bag estimate of error rates 3.3 %) was trained for all treatments on eight representatively chosen sub-volumes (200 × 200 × 200 voxels) that capture the range of structural features found in the X-ray images.

To avoid sampling artifacts (i.e., disturbances from sampling around the column walls and close to the sample top and bottom), only the central part of the soil cores was further analyzed. A cylinder (height = 350 voxels) was cropped 50 voxels below the sample surface, excluding the top and bottom of the sample. A hollow cylinder with a wall diameter of 100 voxels was removed to minimize the impact of disturbances occurring close to the column wall during sampling (c.f. Carr et al., 2020). The final sub-volume had a size of ca. 98 cm^3.

In the next steps the material classes were analyzed using the *PoreSpaceAnalyzer* in SoilJ which implements several MorphoLibJ routines (Legland et al., 2016)

Apart from imaged porosity we also show the imaged pore size distribution, defined as the largest sphere that can fit within the pore structure (Legland et al., 2016). Tube like pores were extracted following the algorithm published in Lucas et al. (2022). We refer to these pores as biopores in the following. The threshold for minimum vesselness, a function estimating a probability-like value to distinguish tube shapes from blob-like structures (Frangi et al., 1998), was set to 0.6. The minimum biopore length was set to 60 voxels. With these settings we aim to focus on larger biopores that might be related to earthworm activity and likely influenced by past or present root activity. Moreover, we determined Γ which is a dimensionless local connectivity measure, confined to the range [0,1] indicating the connectivity probability of given pore clusters (Renard and Allard, 2013; Schlüter et al., 2014). We also checked if the imaged pore space was percolating, i.e., if at least one pore cluster connects top and bottom of the selected region of interest (ROI). We decided to calculate the anisotropy (A) focussing on platy structures perpendicular to z (Equation (1)) as platy structures can be expected after compaction.

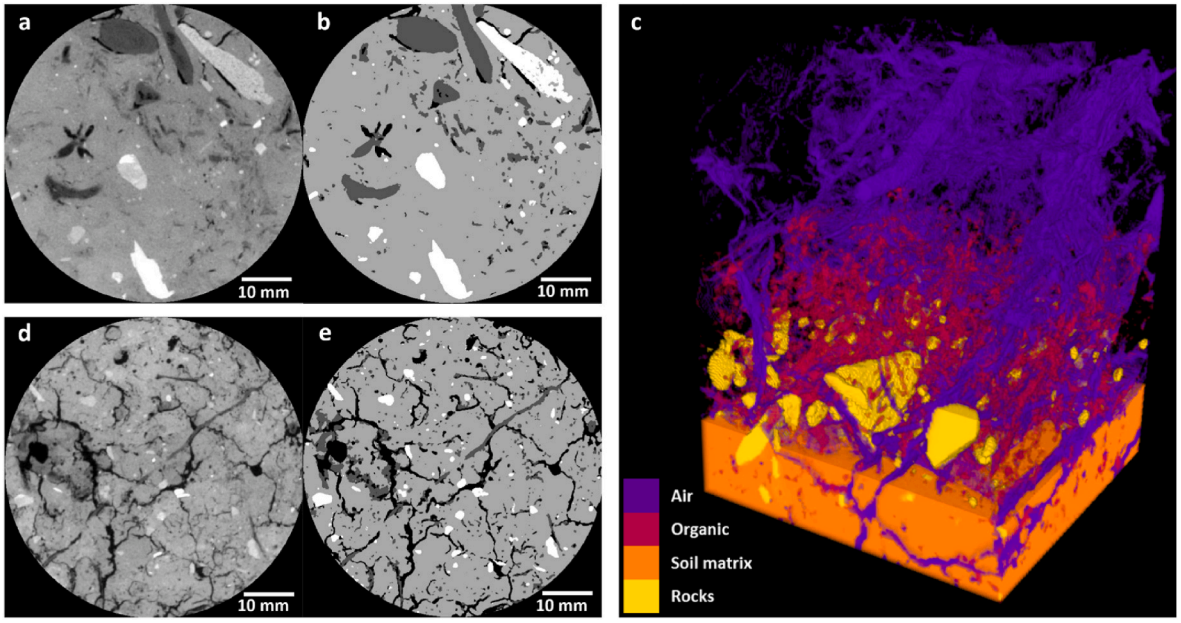

Fig. 2. Image segmentation; a) freshly compacted soil, calibrated greyscale image; b) freshly compacted soil, segmented into four phases (from dark to bright: air, organic, soil matrix, rock fragments); c) 3D illustration of segmented image of uncompacted soil (35.0 × 33.2 × 45.1 mm); d) uncompacted soil, calibrated greyscale image; e) uncompacted soil segmented into four phases.

$$A = \frac{z}{0.5(x+y)+\epsilon} \quad (1)$$

with x, y and z being the count of changes in material class in a binary image in the respective direction. We also introduced a correction factor (ϵ; with $\epsilon = 0$ if $x + y > 0$ and $\epsilon = 1$ if $x + y = 0$) in case of perfect perpendicular alignment of structures towards z. ϵ can be set to 0 in soil as perfect anisotropy is not to be expected. The larger A the stronger the soil structure is layered in the horizontal direction (*platyness*). A value of 1 indicates complete isotropy, values smaller than 1 a predominantly vertical structure.

2.5. Statistical analyses

All statistical analysis were conducted using R (R Core Team, 2025). For the earthworm data generalized linear mixed models (GLMM) were fitted to test the proposed hypotheses. This choice was driven by the nature of the response variable, which consisted of count and positive continuous data with a preponderance of zero observations. The GLMM framework is well-suited for such data structures, as it allows for the specification of an appropriate distribution to model outcomes while effectively addressing issues such as overdispersion and zero inflation. The treatment effect on both earthworm abundance (individuals (ind.) m^{-2}) and biomass (g m^{-2}) was tested, including pH as additional explanatory variable for all earthworms, burrowing earthworms and intermediate earthworms. For litter dwellers, pH was excluded, following the reasoning of Desie et al. (2020) who argued that they (i) do not (primarily) inhabit the soil and (ii) are less sensitive to low pH-values. Due to their high flexibility and the capacity to handle exact zeros, we used GLMMs based on Tweedie exponential dispersion models with an index parameter $1 < \xi < 2$ (Dunn et al., 2018), available in the R-package *glmmTMB* (Brooks et al., 2017). Model assumptions were visually checked using *DHARMa* (Hartig, 2024). If diagnostic plots indicated a violation of assumptions, an additional zero inflation term was added.

In cases of zero variance in one treatment (i.e., all observations were zeros), a paired Wilcoxon test was used to compare the respective treatments. The p-values resulting from the Wilcoxon tests were not adjusted (Nakagawa, 2004) as only clearly pre-defined hypotheses were tested (Midway et al., 2020), each addressing separate research questions (García-Pérez, 2023): (i) the effect of timber harvesting after <1 year, (ii) the effect after 18 years, and (iii) recovery (comparison H01 vs H18). Further details on models and tests are provided in the supplements (Supplement 2).

For data obtained from soil cores in the laboratory and through X-ray imaging, a similar approach was used, with the key difference that a linear mixed model (LMM) using the *nlme* package (Pinheiro et al., 2025; Pinheiro and Bates, 2000) was fitted instead of a GLMM. Initially, models were constructed with a maximal random effects structure (Barr et al., 2013), accounting for varying intercepts between pairs (trafficked/untrafficked) and between soil pits within pairs. However, such maximal models cause a substantial loss of statistical power if the true variance component is small, potentially even resulting in singularity issues (Matuschek et al., 2017).

To address this, model selection based on the corrected Akaike Information Criterion AICc (Hurvich and Tsai, 1989) favored a simpler random effects structure. All LMMs retained soil pit as the only random effect, accounting for baseline variability at the site and enabling a robust analysis of the variables of interest. Model assumptions were evaluated visually using diagnostic plots. In cases where the assumption of homoscedasticity was violated, an additional term was included to allow for different variances between treatments. Due to singularity issues, a simple linear model was used for pH. Further details on the final models can be found in the supplements (Supplement 3).

The comparison of the relevant treatments (C01 vs H01, C18 vs H18 and H01 vs H18) was conducted using the *emmeans* package (Lenth, 2025). As C01 and C18 were sampled from the same population and intended to capture small-scale heterogeneity in soil properties, both controls were not tested against each other.

As texture was only measured on one selected soil core per pit and was not normally distributed, differences were checked using the Kruskal-Wallis test, to investigate potential differences in texture between treatments.

3. Results

3.1. Earthworm abundance and biomass severely reduced in fresh skid trails but higher in old trails

Earthworms also show a general pattern across all functional groups: while (almost) no earthworms were found on H01, old skid trails (H18) showed a higher abundance (ind. m^{-2}) and biomass (g m^{-2}) of earthworms compared to C18 (Fig. 3). Due to non-normality of the data, earthworm results are presented as medians, unless indicated otherwise.

Total earthworm (sum of all individuals from all functional groups) abundance and biomass shows this pattern with a median of zero for both abundance and biomass on H01 (compared to ind. 52 m^{-2} and 28.9 g m^{-2} on C01; $p < 0.01$ for abundance and biomass). On H18, earthworm abundance was significantly higher than for C18 (162 ind. m^{-2} and 28.9 g m^{-2} compared to 27 ind. m^{-2} and 14.6 g m^{-2}; $p = 0.01$ for abundance and $p = 0.13$ for biomass). The difference between H01 and H18 was significant ($p < 0.01$, for both, abundance and biomass) as well.

The intermediate functional group pronouncedly follows the pattern described above. Zero earthworms were found on H01, compared to 15 ind. m^{-2} and 1.8 g m^{-2} for C01 ($p = 0.02$ for both, abundance and biomass). On H18, significantly more earthworms were found than on C18 (64 ind. m^{-2} and 15.6 g m^{-2} compared to 4 ind. m^{-2} and 0.5 g m^{-2}; $p = 0.04$ for abundance and $p = 0.02$ for biomass). Differences between H18 and H01 were significant too ($p < 0.01$ for both, abundance and biomass).

The burrower functional group slightly deviate from this pattern with no significant difference between H18 and C18 for biomass (14.1 g m^{-2} vs 10.3 g m^{-2}; $p = 0.46$), while the difference for abundance is significant (61 ind. m^{-2} vs 4 ind. m^{-2}; $p < 0.01$). H01 again shows a median of zero for both, abundance and biomass compared to 19 ind. m^{-2} and 14.6 g m^{-2} for C01 ($p < 0.01$ for both, abundance and biomass). The difference between H01 and H18 is pronounced again ($p < 0.01$ for both, abundance and biomass).

Very few litter dwellers were encountered throughout all treatments. Except for H18 (4 ind. m^{-2} and 0.4 g m^{-2}) all medians for abundance and biomass showed zero. Only the differences between H01 and H18 were significant (abundance: $p < 0.01$; biomass: $p = 0.02$).

Further details on statistical models, tests, and diagnostics described in this section can be found in the supplements (Supplement 2).

3.2. Laboratory results show treatment effect on bulk density and pH

As expected, soil texture did not show significant differences between treatments, with means of 60.1 % clay and 38.6 % silt at 5 cm depth, and 59.8 % clay and 38.9 % silt at 15 cm depth (Table 1), indicating overall homogeneous site conditions. The clay mineral composition showed no differences between sampling pits, with no indications of clay translocation within the profile. The main components of the clay fraction are kaolinite, followed by illite and vermiculite, as a swelling clay mineral. Vermiculite is part of a mixed-layer mineral, with two different types identified: vermiculite-illite and chlorite-illite. Chlorite is detectable only in traces. Due to the mixed layers, quantification by measuring peak areas was not reliably feasible, so only relative quantities were derived (data and a labeled example diffractogram are provided in the supplements (Supplement 4 & 5)).

The SOC-concentration and the C/N ratio did not show significant

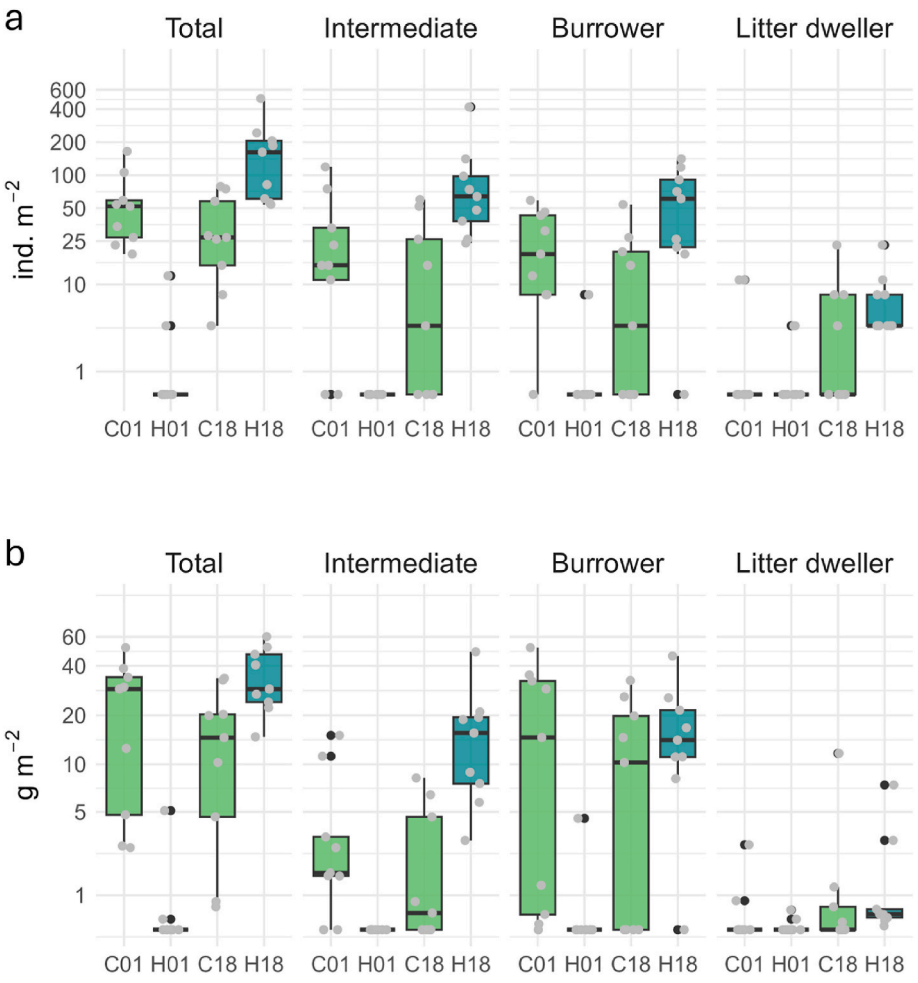

Fig. 3. Earthworm abundance [ind. m^{-2}] (a) and earthworm biomass [g m^{-2}] (b); n = 9 per treatment; H01 was trafficked <1 year before sampling, H18 18 years before sampling. C01 and C18 are the respective controls.

Table 1
Soil properties; bulk density (BD) [g cm^{-3}], clay (<2 μm) [%], silt (63–2 μm) [%], soil organic carbon (SOC) [%] and carbon-to-nitrogen-ratio (C/N) [-]; n = 9 per treatment and depth for BD, SOC and C/N, n = 3 per treatment and depth for soil texture; H01 was trafficked <1 year before sampling, H18 18 years before sampling. C01 and C18 are the respective controls. Lower-case letters indicate significant ($p < 0.05$) differences between trafficked treatments and the respective control; upper-case letters indicate significant differences between recently trafficked (H01) and old skid trails (H18).

Soil property	Depth [cm]	C01		H01		C18		H18	
BD [g cm^{-3}]		$\bar{x}$	*s*	$\bar{x}$	*s*	$\bar{x}$	*s*	$\bar{x}$	*s*
	5	0.99^{a}	0.08	1.31^{b}	0.12	1.00	0.11	1.09	0.22
	15	1.09^{a}	0.13	1.42^{b}	0.09	1.03^{a}	0.07	1.28^{b}	0.10
Clay [%]	5	61.6	5.9	59.8	3.0	59.4	1.3	59.7	1.1
	15	58.5	3.5	61.2	3.6	59.7	1.2	59.9	0.6
Silt [%]	5	36.9	6.9	38.8	3.1	39.4	1.7	39.1	0.7
	15	40.0	4.3	37.4	3.9	39.2	1.2	39.0	0.5
SOC [%]	5	4.74	0.93	3.73	0.89	4.96	0.68	5.57	1.92
	15	3.46	0.84	2.23	0.56	3.83	0.43	3.27	1.10
C/N [-]	5	12.28	1.91	11.44	0.78	11.44	0.54	12.14	0.70
	15	11.05	1.34	9.64	0.80	10.89	0.52	10.29	1.03

differences between treatments, although there is a tendency for higher SOC concentrations at 5 cm depth for H18 and lower concentrations for H01 (Table 1). The pH measured (0–20 cm) showed a clear treatment effect. Both references, C01 and C18, had significantly lower pH values (4.8 ± 0.2 and 4.8 ± 0.1, respectively; $p < 0.01$ for each) than the trafficked treatments H01 and H18 (5.2 ± 0.4 and 5.3 ± 0.4, respectively). No significant difference between H01 and H18 ($p = 0.69$) was detected.

Bulk density (BD) follows the generic pattern described above (Table 1; Fig. 4). However, the variance at 5 cm depth was high, especially for H18, resulting in lower but not statistically significant BD values for H18 compared to H01 ($p = 0.06$). No significant differences between C18 and H18 ($p = 0.41$) were detected. At 15 cm depth, both treatments H01 and H18 have significantly higher bulk densities than their controls ($p < 0.01$ for each), while BD at H18 is not significantly lower than H01 ($p = 0.07$). Further details on statistical models, tests, and diagnostics described in this section can be found in the supplements (Supplement 3).

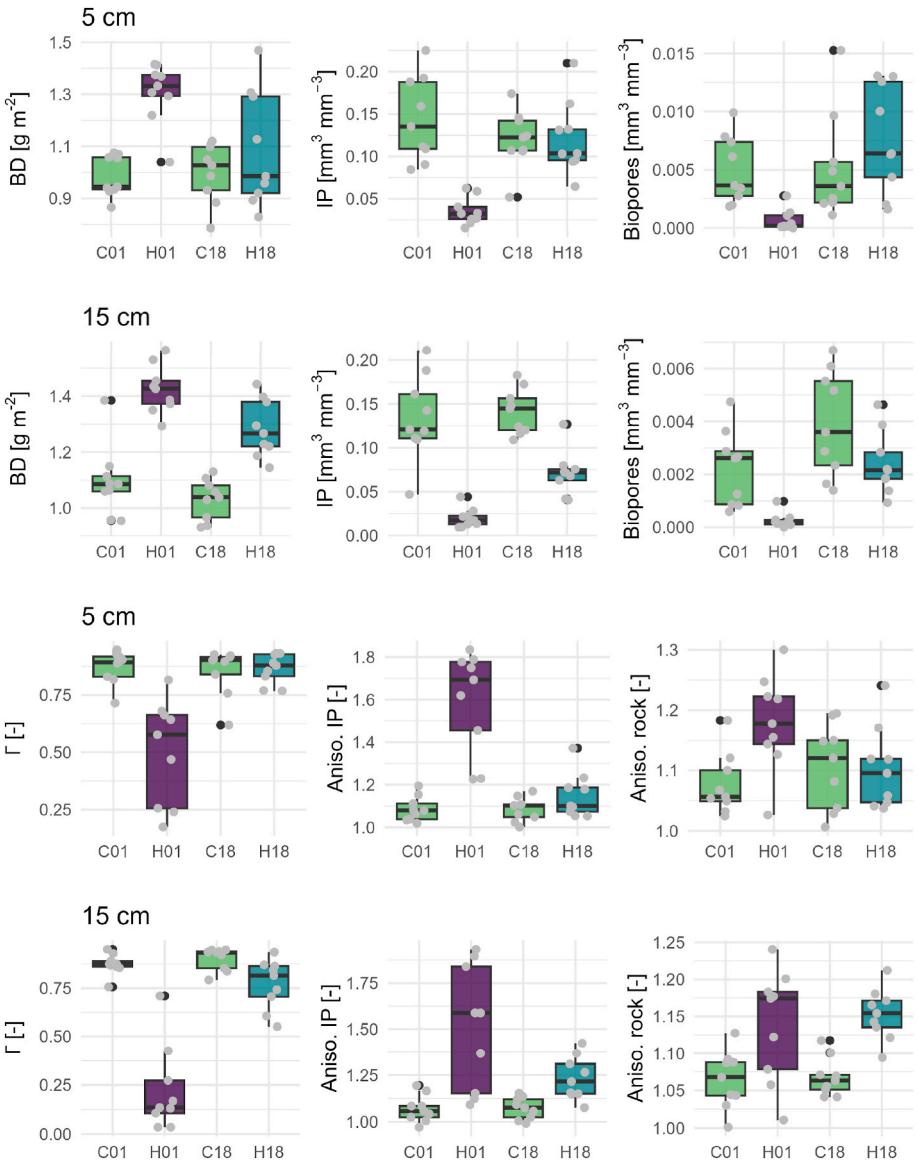

Fig. 4. Overview of parameters from soil sampling and X-ray imaging; Results from bulk density (BD), imaged porosity (IP), biopore porosity (Biopores), connectivity probability Γ [-], anisotropy of imaged pores (Aniso. IP [-]) and anisotropy of rock fragments (Aniso. rock [-]) are displayed; n = 9 per treatment and depth; H01 was trafficked <1 year before sampling, H18 was trafficked 18 years before sampling. C01 and C18 are the respective controls.

3.3. X-ray imaging reveals strong treatment effects on soil structure

An overview of parameters derived from X-ray imaging can be found in Supplement 1 Table S1 and Fig. 4. Imaged porosity is tightly correlated with BD (Fig. 5b; $R^2 = 0.62$) and perfectly follows the general pattern described above. C01 has significantly higher imaged porosity than H01, as does H18 compared to H01 ($p < 0.01$ for both). No difference was observed between C18 and H18 ($p = 0.94$) at 5 cm. At 15 cm depth, all comparisons resulted in significant differences: imaged porosity is higher in both controls compared to H01 and H18 ($p < 0.01$ for both), and imaged porosity at H18 is higher than at H01 ($p = 0.01$).

The imaged pore size distribution shows clear differences between treatments. There is a strong reduction in the dominant pore sizes for H01 compared to C01, while at 5 cm depth, differences between C18 and H18 are not clear. At 15 cm depth, the difference between C18 and H18 is apparent, with the effect of H01 being even more pronounced (Fig. 5a).

Biopores show significant differences with C01 > H01 ($p = 0.02$) and H18 > H01 ($p < 0.01$) at 5 cm depth. No significant differences were observed between C18 and H18 ($p = 0.33$), although H18 appears to have slightly larger bioporosity than C18 (0.77 ± 0.46 % compared to 0.52 ± 0.46 %). At 15 cm depth, significant differences were found with C01 > H01 and H18 > H01 ($p < 0.01$), while the larger number in biopores for C18 compared to H18 were not significant ($p = 0.09$).

Γ-connectivity showed the same pattern: C01 > H01 and H18 > H01 ($p < 0.01$ for both), and no significant differences between C18 and H18 ($p = 0.80$) at 5 cm. At 15 cm depth, all comparisons resulted in significant differences, with lower values for H01 and H18 compared to C01 and C18 ($p < 0.01$ for both), and higher values for H18 versus H01 ($p < 0.05$).

Nine out of 36 samples were not percolating deduced from imaged porosity, meaning no connection between the top and bottom of the ROI existed. All non-percolating samples were from H01, predominantly at 15 cm depth. Fig. 5c shows that until a certain imaged porosity, most pores are part of the percolating pore cluster. Below an imaged porosity of approximately 4 %, there is less connectivity between pore clusters. The average percolation threshold is reached at an imaged porosity of 1.7 ± 0.6 %. Again, differences between treatments followed the general

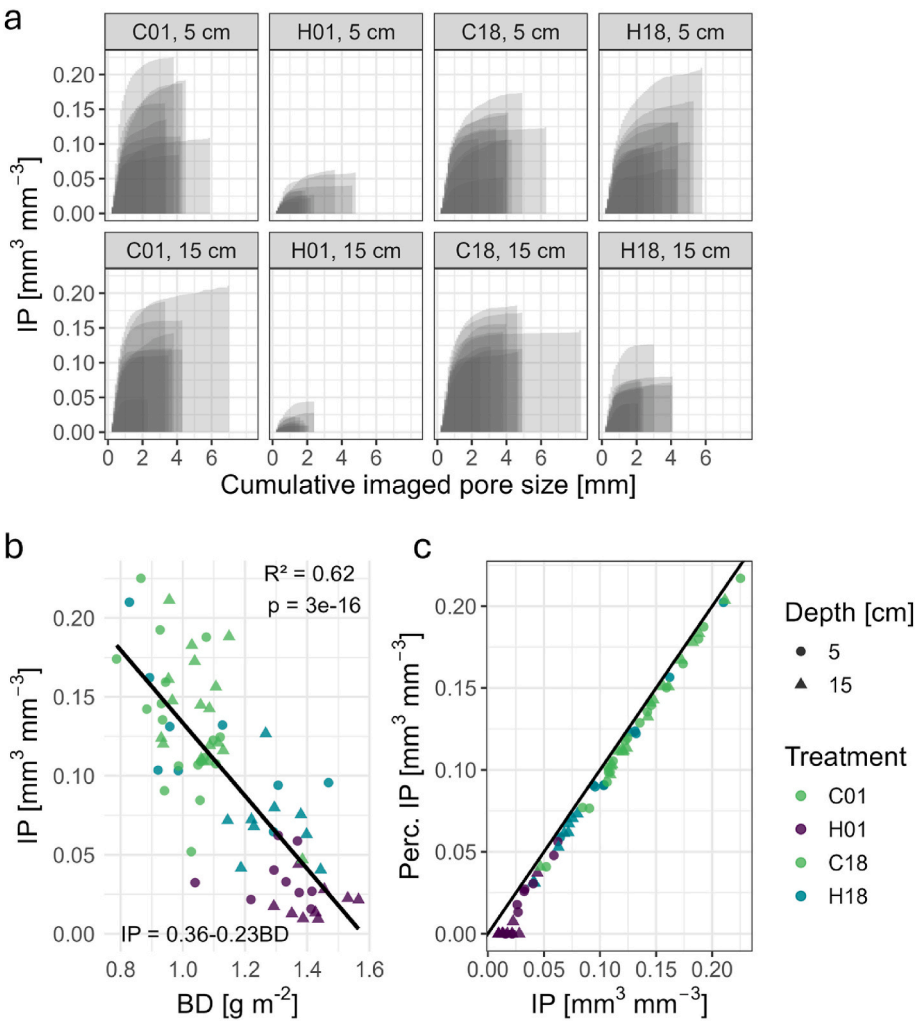

Fig. 5. Imaged porosity; a) cumulative pore size distribution; b) linear regression of imaged porosity (IP) and bulk density (BD); c) percolating imaged porosity (Perc. IP) vs. imaged porosity (IP). H01 was trafficked <1 year before sampling, H18 18 years before sampling. C01 and C18 are the respective controls.

pattern of C01 > H01 and H18 > H01 ($p < 0.01$ for both), with no significant difference between C18 and H18 ($p = 0.93$) at 5 cm. At 15 cm depth, we showed that C01 > H01 and H18 > H01 ($p < 0.01$ for both). The difference between H01 and H18 was significant ($p = 0.02$), with a higher share of percolating pores for H18.

The anisotropy of imaged pores at 5 cm depth is significantly higher in H01 compared to H18 and C01 ($p < 0.01$ for both). The difference between C18 and H18 is not significant ($p = 0.19$). However, at a depth of 15 cm, this difference becomes significant ($p = 0.03$), with H18 showing higher anisotropy. C01 exhibits significantly lower anisotropy than H01 at 15 cm ($p < 0.01$). Due to high variability in H01, the anisotropy in H18 is slightly lower than in H01 but does not reach statistical significance ($p = 0.06$).

The anisotropy of rock fragments (i.e., the alignment of loose rock fragments within the soil core) at 5 cm does not show any significant differences, although a tendency of higher anisotropy for H01 compared to all other treatments can be observed. At 15 cm depth, both treatments H01 and H18 show significantly higher anisotropy compared to their controls ($p = 0.04$ and $p = 0.01$, respectively). No differences between H01 and H18 are observed ($p = 0.63$).

Further details on statistical models, tests, and diagnostics described in this section can be found in the supplements (Supplement 3).

4. Discussion

The mull humus dynamic at our site indicates high faunal activity, which is reflected in the dominance of burrowing and intermediate earthworms and the low abundance of litter dwellers. Slightly higher numbers of litter dwellers were recorded only in the ruts of old skid trails (H18), where more litter had accumulated.

We observed a stark decline or near eradication of earthworms in newly established skid trails. This is followed by a partial recovery of earthworm populations, leading to the highest abundance of earthworms in old skid trails. Coinciding with this our results revealed two consistent patterns across most measured soil parameters: (1) a strong impact of compaction in skid trails within the first year after timber harvesting, and (2) a depth-dependent trend in recovery, with full recovery observed at 5 cm and only partial recovery at 15 cm after 18 years (Table 1; Supplement 1 Table S1; Fig. 4).

4.1. Immediate impact of compaction

Similar to previous research (Bottinelli et al., 2014a; Jordan et al., 1999) and in agreement with our hypothesis, we observed a significant immediate decline in all functional earthworm groups following timber harvesting–induced soil compaction. Single individuals of the burrower and litter dweller group were found, while no intermediate individuals were detected. This is consistent with the fact that endogeic species are

less mobile compared to their epigeic and anecic counterparts (Chatelain and Mathieu, 2017). As mentioned above (2.2 Earthworm sampling and analyses), the two intermediate species were initially classified as endogeic species (Bouché, 1972). Interestingly, Bottinelli et al. (2014a) still found a low abundance of endogeic species directly after timber harvesting, concluding they might be less sensitive towards compaction. However, this difference to our results is likely due to a lower trafficking intensity at their experimental site (1 compared to 6–10 machine cycles). The higher trafficking intensity observed in our experiment reflects typical conditions in the main sections of a systematic skid trail network, particularly those closer to the log landing (DeArmond et al., 2021).

Chemical and biological conditions at our site remained suitable for earthworms after trafficking – particularly with an observed increase in pH. This initial increase in pH likely results from the exposure of deeper soil layers and the development of anaerobic conditions caused by compaction. The resulting decrease in redox potential is known to elevate pH levels (Husson, 2013). Under these reducing conditions, compacted environments promote the activity of sulfur- and metal-reducing microbes (Hartmann et al., 2014), which consume protons during the reduction of iron and manganese oxides. These microbial processes are often reflected in the appearance of greyish mottling in the topsoil (Klein-Raufhake et al., 2024). However, while these processes contribute to the increase in pH, the physical effects of compaction simultaneously created unfavorable conditions that inhibited earthworm activity.

The well-established loss of macropores as an immediate effect of timber harvesting-induced compaction (e.g., Behringer et al., 2025; Greacen and Sands, 1980; McNabb et al., 2001) is clearly reflected in our data and confirms our hypothesis. The strong linear correlation between imaged porosity and bulk density (Fig. 5b) suggests that compaction primarily occurs within the pore size range captured by X-ray imaging.

Hansson et al. (2018), who used similar methods to study silt loam soils in the boreal zone, found comparable results: undisturbed samples showed most pore space connected within a single cluster, whereas compacted samples exhibited reduced pore connectivity (Fig. 5c).

However, compared to Hansson et al. (2018) the compaction effects on our study site (a clay soil in the temperate zone) were even more pronounced. While most compacted samples in Hansson et al. (2018) remained percolating, a substantial portion of our compacted samples did not. Differences in image resolution could partially explain this observation. However, saturated hydraulic conductivity values of compacted samples (H01) from our site (Behringer et al., 2025) were over an order of magnitude lower than those reported by Hansson et al. (2018). This supports the conclusion that both porosity and connectivity are more severely reduced in our study area.

Similarly, Bottinelli et al. (2014b) reported a strong immediate reduction in macroporosity on a silt loam temperate forest soil, with decreases of 93 % at 0–7 cm and 68 % at 15–30 cm depth. These values are comparable to our observed reductions of 75 % at 5 cm and 85 % at 15 cm, despite differences in soil texture (clay vs. silt loam).

Overall, our findings align with observations from agricultural research, which similarly report compaction-induced losses in pore connectivity and increased anisotropy (Pöhlitz et al., 2019). The high variance we observed, particularly in the anisotropy of imaged pores at 15 cm depth, might be related to the distribution of horizontal cracks in this treatment. While some samples intersected larger horizontal crack structures, others may not include any major (horizontal) structures, resulting in lower anisotropy values. In our study, higher anisotropy indicates the formation of horizontally aligned, platy structures, which may promote preferential lateral water flow (Beck-Broichsitter et al., 2022). Yet, despite this, low infiltration rates suggest that surface runoff remains the dominant hydrological process on skid trails at our site (Behringer et al., 2025). Moreover, these horizontal structures, together with reduced pore connectivity, impede gas exchange (Frey et al., 2009), as reflected in hydromorphic features such as mottling observed in compacted areas (Behringer et al., 2025; Klein-Raufhake et al., 2024; Startsev and McNabb, 2009). These altered soil physical conditions are linked to changes in the greenhouse gas balance of forest soils, with elevated N_2O emissions and decreased CH_4 uptake (Teepe et al., 2004).

4.2. Higher earthworm abundance in 18-year-old skid trails

Old skid trails appear to have developed into a new habitat, offering conditions suitable for earthworms. Similar to natural pit-and-mound structures, which support higher soil organic carbon (SOC), soil moisture, and earthworm abundance and biomass (Kooch et al., 2014), old skid trails exhibit characteristics that favor earthworm activity. Beech litter accumulates in the concave profile of old ruts, providing an abundant food source for earthworms. This is supported by a trend of higher SOC concentrations at 5 cm depth in old skid trails (5.6 ± 1.9 %) compared to control plots (5.0 ± 0.7 %), suggesting the incorporation of litter into the soil, which benefits soil-feeding species. Ruts retain higher soil moisture (Hansson et al., 2019) with elevated moisture levels persisting even in recovered layers due to water stagnation caused by compacted deeper soil layers (DeArmond et al., 2023). Old skid trails also exhibit higher pH values, which further enhance conditions for earthworms. The accumulation of beech litter, known for its relatively high pH and Ca^{2+} concentrations (Kupka and Gruba, 2022) might contribute to higher pH-values adding to the increases due to altered redox conditions discussed earlier (4.1 Immediate impact of compaction). Moreover, earthworm activity itself may create a positive feedback loop, where their activity promotes forest floor turnover, increases topsoil pH, and creates favourable living conditions (Desie et al., 2020).

Coinciding with these favourable conditions we observed a significantly higher abundance of earthworms in old skid trails, along with a trend toward higher biomass. This indicates that earthworms were able to recolonize highly compacted forest soils, although full recovery to the untrafficked state was not achieved.

For intermediate species, both abundance and biomass were significantly higher in old skid trails compared to untrafficked plots. Ampoorter et al. (2011) similarly reported a higher abundance of endogeic earthworms in skid trails within three years after trafficking, likely due to increased pH and soil moisture. However, other studies have documented incomplete earthworm recovery in temperate forests even after 20–25 years (Sohrabi et al., 2020a, 2020b, 2022), underscoring the context-dependent nature of ecological recovery processes.

For burrowers, we observed a different pattern compared to the intermediate group. While significantly more individuals were found in old skid trails than in control plots, no differences in biomass were detected. This suggests that control plots provide habitat for a few large adult individuals, whereas old skid trails are dominated by smaller juvenile individuals (Supplement 2: Earthworm Models; 4.3.3). Juveniles have been reported to colonize new habitats (Capowiez et al., 2000). However, it seems improbable that burrowing individuals, such as *Dendrobaena depressa*, would require 18 years to establish, especially given that other functional groups did not exhibit a similar pattern. Additionally, the recovered structure of the topsoil suggests biological activity has been reestablished for some time.

We hypothesize that the observed pattern reflects differing habitat preferences and potentially even territorial behaviour (as observed for other species (Capowiez and Belzunces, 2001)) between adult and juvenile individuals of *Dendrobaena depressa*. Due to different morphological features, i.e. thicker pre-clitellar epidermis (Briones and Álvarez-Otero, 2018), adult earthworms inhabit different ecological niches than juvenile earthworms. In burrowing species, juvenile individuals are typically found at shallower depths (Gerard, 1967; Rundgren, 1975). This pattern aligns with the observed recovery of soil structure at 5 cm depth, while deeper layers still exhibited signs of compaction. Adult individuals, which burrow deeper (Zicsi et al., 2011) likely avoid rut habitats, due to their preference for uncompacted soil (e.g., Bottinelli et al., 2014a; Capowiez et al., 2021; Ducasse et al., 2021).

For juvenile *Dendrobaena depressa*, however, the recovered topsoil in these ruts may offer more favourable conditions.

4.3. Pronounced depth gradient in soil recovery

In contrast to agricultural systems, where mechanical interventions like ploughing or tillage can alleviate compaction, most forest soils rely on slow natural processes for recovery. As a result, compaction effects in forest soils are more persistent and long-lasting. At our site, the presence of swelling clay minerals suggests that initial recovery may be driven by swelling and shrinking processes (Diel et al., 2019; Peth et al., 2010) which are known to play a key role in the recovery of skid trails (DeArmond et al., 2021). This may be followed by colonization from hygrophilous plant species such as *Juncus* spp. and *Carex* spp. (Mercier et al., 2019), whose roots further aid in penetrating compacted layers (Bottinelli et al., 2014b). These conditions facilitate the gradual recolonization of earthworms, as hypothesized by Bottinelli et al. (2014a, 2014b). Earthworms, with their ability to burrow through compacted soils (Ducasse et al., 2021; Jégou et al., 2000; Joschko et al., 1989), can further enhance soil structure recovery.

In our study, old skid trails tended to show the greatest number of biopores, corresponding to the greatest earthworm abundance. However, while increased earthworm abundance can enhance pore formation (Ma et al., 2021), the relationship is not necessarily straightforward. For example, endogeic species often refill their burrows with casts (Capowiez et al., 2014; Le Couteulx et al., 2015), potentially obscuring their contribution to pore networks. This effect is likely relevant at our site as all soil-dwelling species (burrowers and intermediate species) identified are known to predominantly cast within the soil (Zicsi et al., 2011).

Capowiez et al. (2021) observed that endogeic species tend to burrow less vertically in compacted soils, and even *Lumbricus terrestris*, known for its deep vertical burrows, significantly reduces burrowing depth under such conditions (Ducasse et al., 2021). This is also reported by Sohrabi et al. (2020b) who showed decreasing earthworm abundance and biomass with increasing depth in old skid trails.

Consistent with the observed behavior of earthworms, our study revealed a pronounced depth gradient in soil structure recovery, including biopores, suggesting an active role of earthworms in the recovery process. At 5 cm depth, soil structure showed full recovery after 18 years, whereas compaction at 15 cm remained significant. This vertical gradient aligns with short-term (2–3 years) recovery patterns reported by Bottinelli et al. (2014b).

Ebeling et al. (2016) documented recovery at 5 cm depth within 10–20 years in similarly clay-rich, biologically active forest soils. Bulk density in our study – recovering to a median of ca.

1.0 g cm^{-3} – closely matched the values found by Ebeling et al. (2016). The variance of the recovered upper soil layer though, is still noticeably higher than in the control. This indicates small-scale heterogeneity in the recovery processes.

Deeper soil layers typically recover slower (Muys, 1989; Page--Dumroese et al., 2006). Wallace et al. (2021) reported incomplete recovery of bulk density after 10 years in a silt loam, likely due to greater sampling depth (0–10 cm). Similarly, DeArmond et al. (2023) observed full recovery at 0–5 cm, but persistent compaction at 5–10 cm, even after 28 years in Amazonian clayey soils – suggesting that compacted sublayers have a continued impact on the layers above. Tavankar et al. (2022) showed that recovery of clay to clay-loam soils (0–10 cm) may take 20–30 years for lightly trafficked sites, and over 30 years for heavily trafficked skid trails. Even higher recovery times were shown for silt loam textured soils with low activity of soil biota, where even after 37 years soil layers below 10 cm depth had not yet fully recovered (Schäffer, 2022). These results highlight that deeper soil layers function as long-term archives of compaction, making assessment depth a critical factor in interpreting soil recovery (DeArmond et al., 2021).

At 15 cm depth, most structural parameters in our study approached intermediate values between untrafficked and recently compacted soils. However, the anisotropy of rock fragments showed no recovery trend. The horizontal alignment of platy rock fragments persisted over time, indicating a lasting structural modification. This persistence may have long-term implications for water and gas transport, as observed by Beck-Broichsitter et al. (2022), who reported that naturally layered bedrock can lead to horizontal pore alignment and lateral preferential flow. These findings suggest that such physical reorganization may continue to influence soil aeration and hydrology long after other indicators of compaction have recovered. Our findings imply that rock fragment anisotropy could serve as a sensitive and long-term indicator of past soil compaction, retaining evidence of mechanical disturbance more effectively than other structural parameters.

While deeper sampling could have provided additional insights into subsoil recovery processes, the high rock fragment content at our site limited representative sampling below 20 cm. Despite this limitation, our findings clearly demonstrate a pronounced depth gradient in soil structure recovery, highlighting the persistent impact of heavy machinery on deeper soil layers (Keller and Or, 2022).

By assessing biopores and earthworm communities, our study provides new insights into the recovery of soil structure and earthworm populations following timber harvesting. However, it does not fully isolate the specific role of earthworms in driving structural recovery. Gasser et al. (in prep.)

working at the same site, observed that tree roots may follow a recovery pattern similar to that of earthworms. Disentangling the contributions of earthworms and roots would require a different experimental design, such as the long-term exclusion of earthworms and/or roots. However, maintaining such an approach over an 18-year period under field conditions would be extremely challenging.

What we did observe is that old skid trails are characterized by a highly biologically active layer sitting atop a hard pan, which continues to influence the conditions above.

4.4. Management implications

The results – particularly those concerning earthworms – are only applicable to conditions where soil-dwelling earthworms are present. At a global scale, earthworm abundance and distribution are primarily driven by climatic variables such as temperature and precipitation (Phillips et al., 2019) and post glacial migration (Hendrix et al., 2008). At a European scale however, soil and litter related factors such as soil pH (Desie et al., 2020; Jänsch et al., 2013) and vegetation type, including tree species composition (Schelfhout et al., 2017), best explain earthworm presence (De Wandeler et al., 2016). In temperate forests with low faunal activity, soil recovery after compaction may be even slower. This is supported by Schäffer (2022), who reported only partial recovery of soil parameters nearly four decades after trafficking.

Our study clearly highlights the long recovery times of skid trails following soil compaction (DeArmond et al., 2021), emphasizing the need for skid trails to be designated as permanent and clearly marked (Picchio et al., 2020), particularly across rotation periods. To reduce the proportion of compacted area, increasing the spacing between skid trails would be beneficial from the perspective of soil conservation. However, widening the spacing between skid trails would necessitate manual felling (with chainsaws) for trees located at greater distances from trails, as the reach of the harvester arm is limited. This may negatively affect occupational safety, operational productivity, and harvesting costs.

Clay soils, including those at our site, are particularly susceptible to compaction (Cambi et al., 2015). Our results underscore the critical importance of implementing mitigation strategies in such areas. Limiting timber harvesting to dry periods is another effective strategy to reduce soil compaction (Grünberg et al., 2025). When this is not feasible, alternative harvesting methods, such as cable yarding, should be considered – not only for steep terrain but also for protecting vulnerable soils, as they have a lower impact on soil structure (Behringer

et al., 2025). Additionally, using animal power (Picchio et al., 2020) or lighter machinery can reduce compaction depth, even when contact stress remains within a similar range (Keller and Or, 2022). Shallower compacted layers are more accessible to biological activity and natural regeneration processes. This can result in less permanent structural damage and enable faster recovery of forest soil ecosystems. Although soil-protective harvesting methods may come with short-term trade-offs, they promote long-term ecosystem resilience by safeguarding soil health and preserving key soil functions like water infiltration, nutrient cycling, and root growth.

5. Conclusion

Our study underscores the significant and long-lasting impacts of timber harvesting on soil structure and earthworm communities – key components of soil health – due to compaction caused by heavy machinery. The recovery of soil structure is slow, with complete recovery at 5 cm depth but persistent compaction effects at 15 cm, highlighting a depth gradient in recovery. We observe a highly biological active layer with recovered pore space sitting on top of a hard pan, that continues to influence the soil conditions above. These findings emphasize the importance of mitigating the effects of heavy machinery through strategic management practices, such as limiting traffic to designated skid trails.

The interaction between soil structure and earthworm communities suggests that earthworms may play a crucial role in the recovery process, although compaction in deeper layers continues to impede full ecological recovery. Our research also indicates that old skid trails, with their altered soil conditions, may provide a novel habitat that fosters higher earthworm abundance and biomass, contributing to gradual soil restoration.

Management strategies should focus on reducing compaction, such as increasing skid trail spacing, employing lighter machinery, and scheduling harvesting during dry periods. While these approaches may initially pose challenges in terms of cost and productivity, they offer substantial long-term benefits by supporting soil functions essential for resilient forest ecosystems.

CRediT authorship contribution statement

Maximilian Behringer: Writing – original draft, Visualization, Supervision, Software, Methodology, Investigation, Formal analysis, Data curation, Conceptualization. **John Koestel:** Writing – review & editing, Validation, Supervision, Software, Methodology, Formal analysis, Conceptualization. **Bart Muys:** Writing – review & editing, Validation, Supervision, Methodology. **Karin Wriessnig:** Writing – review & editing, Supervision, Methodology, Investigation. **Markus Bieringer:** Investigation. **Matthias Schlögl:** Writing – review & editing, Validation, Software. **Klaus Katzensteiner:** Writing – review & editing, Validation, Supervision, Methodology, Funding acquisition, Conceptualization.

Data availability

The data used in this research is available on Zenodo https://doi.org/10.5281/zenodo.15631419. Raw data will be made available on request.

Declaration of generative AI and AI-assisted technologies

During the preparation of this work the authors used DeepL Write and ChatGPT to improve language and readability. After using these tools, the authors reviewed and edited the content as needed and take full responsibility for the content of the publication.

Funding

Funded by the Austrian Forest Fund with support from the Federal Ministry of Agriculture, Forestry, Regions and Water Management, grant number 101724.

Declaration of competing interest

The authors declare that they have no known competing financial interests or personal relationships that could have appeared to influence the work reported in this paper.

Acknowledgements

The field experiments were conducted as part of the HoBo research project, which also supported data collection. We are deeply grateful to Lisa Gasser, Raphael Schatz, Marcus Froemel, David Morgenbesser, Anna Schrötter, Marcel Hirsch, and Natalie Friedl for their invaluable technical assistance during the field campaign and laboratory work. We thank Lisa Gasser, Julian Grünberg and Armin Malli for the insightful discussions. Special thanks are extended to Austrian Federal Forests (ÖBf) for their cooperation and assistance, including facilitating site access, providing records of previous harvests, and connecting us with retired forest operations contractor Johann Hess, whose insights regarding the machinery used during timber harvesting in 2004/05 were invaluable. We are grateful to Agroscope Reckenholz, particularly Maria Vorkauf and Valerio Volpe, for their support in X-ray imaging and image processing. Our gratitude goes to Edith Gruber for validating our earthworm identification. Lastly, we thank Michaël Hedde and Yvan Capowiez for their insightful comments on the functional grouping of earthworms. Open access funding provided by BOKU University.

Appendix A. Supplementary data

Supplementary data to this article can be found online at https://doi.org/10.1016/j.soilbio.2025.109953.

References

Ampoorter, E., De Schrijver, A., De Frenne, P., Hermy, M., Verheyen, K., 2011. Experimental assessment of ecological restoration options for compacted forest soils. Ecological Engineering 37, 1734–1746. https://doi.org/10.1016/j.ecoleng.2011.07.007.

Arrázola-Vásquez, E., Larsbo, M., Capowiez, Y., Taylor, A., Sandin, M., Iseskog, D., Keller, T., 2022. Earthworm burrowing modes and rates depend on earthworm species and soil mechanical resistance. Applied Soil Ecology 178, 104568. https://doi.org/10.1016/j.apsoil.2022.104568.

Austrian Standards, 2006. ÖNORM L 1083 Chemische Bodenuntersuchung – Bestimmung Der Acidität (pH-Wert).

Barr, D.J., Levy, R., Scheepers, C., Tily, H.J., 2013. Random effects structure for confirmatory hypothesis testing: keep it maximal. Journal of Memory and Language 68, 255–278. https://doi.org/10.1016/j.jml.2012.11.001.

Beck-Broichsitter, S., Dusek, J., Vogel, T., Horn, R., 2022. Anisotropy of soil water diffusivity of hillslope soil under spruce forest derived by X-ray CT and lab experiments. Environmental Earth Sciences 81, 457. https://doi.org/10.1007/s12665-022-10511-9.

Behringer, M., Grünberg, J., Katzensteiner, K., Kitzler, B., Kohl, B., Lechner, V., Malli, A., Markart, G., Meißl, G., Scheidl, C., 2025. Comparison of the effect of winch-assisted timber harvesting systems and cable yarding on soil water retention and surface runoff in a temperate deciduous forest. Journal of Hydrology, 133183. https://doi.org/10.1016/j.jhydrol.2025.133183.

Bellabarba, A., Giagnoni, L., Adessi, A., Marra, E., Laschi, A., Neri, F., Mastrolonardo, G., 2024. Short-term machinery impact on microbial activity and diversity in a compacted forest soil. Applied Soil Ecology 203, 105646. https://doi.org/10.1016/j.apsoil.2024.105646.

Berg, S., Kutra, D., Kroeger, T., Straehle, C.N., Kausler, B.X., Haubold, C., Schiegg, M., Ales, J., Beier, T., Rudy, M., Eren, K., Cervantes, J.I., Xu, B., Beuttenmueller, F., Wolny, A., Zhang, C., Koethe, U., Hamprecht, F.A., Kreshuk, A., 2019. Ilastik: interactive machine learning for (bio)image analysis. Nature Methods 16, 1226–1232. https://doi.org/10.1038/s41592-019-0582-9.

Beylich, A., Oberholzer, H.-R., Schrader, S., Höper, H., Wilke, B.-M., 2010. Evaluation of soil compaction effects on soil biota and soil biological processes in soils. Soil and Tillage Research 109, 133–143. https://doi.org/10.1016/j.still.2010.05.010.

Bottinelli, N., Capowiez, Y., Ranger, J., 2014a. Slow recovery of earthworm populations after heavy traffic in two forest soils in northern France. Applied Soil Ecology 73, 130–133. https://doi.org/10.1016/j.apsoil.2013.08.017.
Bottinelli, N., Hallaire, V., Goutal, N., Bonnaud, P., Ranger, J., 2014b. Impact of heavy traffic on soil macroporosity of two silty forest soils: initial effect and short-term recovery. Geoderma 217–218, 10–17. https://doi.org/10.1016/j.geoderma.2013.10.025.
Bottinelli, N., Hedde, M., Jouquet, P., Capowiez, Y., 2020. An explicit definition of earthworm ecological categories – marcel Bouché's triangle revisited. Geoderma 372, 114361. https://doi.org/10.1016/j.geoderma.2020.114361.
Bouché, M., 1972. Lombriciens De France, Ecologie Et Systématique. INRA, Paris. Annales de Zoologie–Ecologie animale.
Brindley, G.W., Brown, G., 1982. Crystal Structures of Clay Minerals and Their X-ray Identification. The Mineralogical Society of Great Britain and Ireland.
Briones, M.J.I., Álvarez-Otero, R., 2018. Body wall thickness as a potential functional trait for assigning earthworm species to ecological categories. Pedobiologia 67, 26–34. https://doi.org/10.1016/j.pedobi.2018.02.001.
Brooks, M.E., Kristensen, K., Benthem, K.J. van, Magnusson, A., Berg, C.W., Nielsen, A., Skaug, H.J., Maechler, M., Bolker, B.M., 2017. glmmTMB balances speed and flexibility among packages for zero-inflated generalized linear mixed modeling. The R Journal 9, 378–400.
Cambi, M., Certini, G., Neri, F., Marchi, E., 2015. The impact of heavy traffic on forest soils: a review. Forest Ecology and Management 338, 124–138. https://doi.org/10.1016/j.foreco.2014.11.022.
Capowiez, Y., Belzunces, L., 2001. Dynamic study of the burrowing behaviour of Aporrectodea nocturna and Allolobophora chlorotica : interactions between earthworms and spatial avoidance of burrows. Biology and Fertility of Soils 33, 310–316. https://doi.org/10.1007/s003740000327.
Capowiez, Y., Bottinelli, N., Jouquet, P., 2014. Quantitative estimates of burrow construction and destruction, by anecic and endogeic earthworms in repacked soil cores. Applied Soil Ecology 74, 46–50. https://doi.org/10.1016/J.APSOIL.2013.09.009.
Capowiez, Y., Marchán, D., Decaëns, T., Hedde, M., Bottinelli, N., 2024. Let earthworms be functional - definition of new functional groups based on their bioturbation behavior. Soil Biology and Biochemistry 188, 109209. https://doi.org/10.1016/j.soilbio.2023.109209.
Capowiez, Y., Pierret, A., Monestiez, P., Belzunces, L., 2000. Evolution of burrow systems after the accidental introduction of a new earthworm species into a Swiss pre-alpine meadow. Biology and Fertility of Soils 31, 494–500. https://doi.org/10.1007/s003740000198.
Capowiez, Y., Sammartino, S., Keller, T., Bottinelli, N., 2021. Decreased burrowing activity of endogeic earthworms and effects on water infiltration in response to an increase in soil bulk density. Pedobiologia 85–86, 150728. https://doi.org/10.1016/j.pedobi.2021.150728.
Carr, S.J., Diggens, L.M., Spencer, K.L., 2020. There is no such thing as 'undisturbed' soil and sediment sampling: sampler-induced deformation of salt marsh sediments revealed by 3D X-ray computed tomography. Journal of Soils and Sediments 20, 2960–2976. https://doi.org/10.1007/s11368-020-02655-7.
Chatelain, M., Mathieu, J., 2017. How good are epigeic earthworms at dispersing? An investigation to compare epigeic to endogeic and anecic groups. Soil Biology and Biochemistry 111, 115–123. https://doi.org/10.1016/j.soilbio.2017.04.004.
Christian, E., Zicsi, A., 1999. A synoptic key to the earthworms of Austria (oligochaeta: lumbricidae). Bodenkultur 50, 121–131.
De Wandeler, H., Sousa-Silva, R., Ampoorter, E., Bruelheide, H., Carnol, M., Dawud, S. M., Dănilă, G., Finer, L., Hättenschwiler, S., Hermy, M., Jaroszewicz, B., Joly, F.-X., Müller, S., Pollastrini, M., Ratcliffe, S., Raulund-Rasmussen, K., Selvi, F., Valladares, F., Van Meerbeek, K., Verheyen, K., Vesterdal, L., Muys, B., 2016. Drivers of earthworm incidence and abundance across European forests. Soil Biology and Biochemistry 99, 167–178. https://doi.org/10.1016/j.soilbio.2016.05.003.
DeArmond, D., Ferraz, J.B.S., De Oliveira, L.R., Lima, A.J.N., Falcão, N.P.D.S., Higuchi, N., 2023. Soil compaction in skid trails still affects topsoil recovery 28 years after logging in central Amazonia. Geoderma 434, 116473. https://doi.org/10.1016/j.geoderma.2023.116473.
DeArmond, D., Ferraz, J.B.S., Higuchi, N., 2021. Natural recovery of skid trails: a review. Can. J. For. Res. 51, 948–961. https://doi.org/10.1139/cjfr-2020-0419.
Desie, E., Van Meerbeek, K., De Wandeler, H., Bruelheide, H., Domisch, T., Jaroszewicz, B., Joly, F., Vancampenhout, K., Vesterdal, L., Muys, B., 2020. Positive feedback loop between earthworms, humus form and soil pH reinforces earthworm abundance in European forests. Functional Ecology 34, 2598–2610. https://doi.org/10.1111/1365-2435.13668.
Diel, J., Vogel, H.-J., Schlüter, S., 2019. Impact of wetting and drying cycles on soil structure dynamics. Geoderma 345, 63–71. https://doi.org/10.1016/j.geoderma.2019.03.018.
Ducasse, V., Darboux, F., Auclerc, A., Legout, A., Ranger, J., Capowiez, Y., 2021. Can Lumbricus terrestris be released in forest soils degraded by compaction? Preliminary results from laboratory and field experiments. Applied Soil Ecology 168, 104131. https://doi.org/10.1016/j.apsoil.2021.104131.
Dunn, P.K., Smyth, G.K., others, 2018. Generalized Linear Models with Examples in R. Springer.
Ebeling, C., Lang, F., Gaertig, T., 2016. Structural recovery in three selected forest soils after compaction by forest machines in Lower Saxony, Germany. Forest Ecology and Management 359, 74–82. https://doi.org/10.1016/j.foreco.2015.09.045.
Flores Fernández, J.L., Rubin, L., Hartmann, P., Puhlmann, H., Von Wilpert, K., 2019. Initial recovery of soil structure of a compacted forest soil can be enhanced by technical treatments and planting. Forest Ecology and Management 431, 54–62. https://doi.org/10.1016/j.foreco.2018.04.045.
Frangi, A.F., Niessen, W.J., Vincken, K.L., Viergever, M.A., 1998. Multiscale vessel enhancement filtering. In: Wells, W.M., Colchester, A., Delp, S. (Eds.), Medical Image Computing and Computer-Assisted Intervention — MICCAI'98, Lecture Notes in Computer Science. Springer, Berlin Heidelberg, Berlin, Heidelberg, pp. 130–137. https://doi.org/10.1007/BFb0056195.
Frey, B., Kremer, J., Rüdt, A., Sciacca, S., Matthies, D., Lüscher, P., 2009. Compaction of forest soils with heavy logging machinery affects soil bacterial community structure. European Journal of Soil Biology 45, 312–320. https://doi.org/10.1016/j.ejsobi.2009.05.006.
García-Pérez, M.A., 2023. Use and misuse of corrections for multiple testing. Methods in Psychology 8, 100120. https://doi.org/10.1016/j.metip.2023.100120.
Gasser, L., Schönauer, M., Otgonsuren, B., Sandén, H., Katzensteiner, K., Douglas, G., Rewald, B., in Prep. Short- and long-term Effects of Mechanized Harvesting: Fine Roots and EM of Fagus sylvatica Recovered in Topsoil but Are Persistently Constrained in Compacted Subsoil Two Decades After Harvesting.
Gerard, B.M., 1967. Factors affecting earthworms in pastures. Journal of Animal Ecology 36, 235. https://doi.org/10.2307/3024.
Greacen, E., Sands, R., 1980. Compaction of forest soils. A review. Soil Research 18, 163. https://doi.org/10.1071/SR9800163.
Grünberg, J., Holzleitner, F., Behringer, M., Gollob, C., Kanzian, C., Katzensteiner, K., Kühmaier, M., 2025. Impacts of a fully mechanized timber harvesting system on soil physical properties after a pronounced dry period. Soil and Tillage Research 251, 106551. https://doi.org/10.1016/j.still.2025.106551.
Hansson, L., Koestel, J., Ring, E., Gärdenäs, A.I., 2018. Impacts of off-road traffic on soil physical properties of forest clear-cuts: X-Ray and laboratory analysis. Scandinavian Journal of Forest Research 33, 166–177. https://doi.org/10.1080/02827581.2017.1339121.
Hansson, L., Šimůnek, J., Ring, E., Bishop, K., Gärdenäs, A.I., 2019. Soil compaction effects on root-zone hydrology and vegetation in boreal forest clearcuts. Soil Science Society of America Journal 83. https://doi.org/10.2136/sssaj2018.08.0302.
Hartig, F., 2024. DHARMa: residual diagnostics for hierarchical (Multi-Level/mixed) regression models. https://doi.org/10.32614/CRAN.package.DHARMa.
Hartmann, M., Niklaus, P.A., Zimmermann, S., Schmutz, S., Kremer, J., Abarenkov, K., Lüscher, P., Widmer, F., Frey, B., 2014. Resistance and resilience of the forest soil microbiome to logging-associated compaction. The ISME Journal 8, 226–244.
Hendrix, P.F., Callaham, M.A., Drake, J.M., Huang, C.-Y., James, S.W., Snyder, B.A., Zhang, W., 2008. Pandora's box contained bait: the global problem of introduced earthworms. Annual Review of Ecology, Evolution and Systematics 39, 593–613. https://doi.org/10.1146/annurev.ecolsys.39.110707.173426.
Hurvich, C.M., Tsai, C.-L., 1989. Regression and time series model selection in small samples. Biometrika 76, 297–307. https://doi.org/10.1093/biomet/76.2.297.
Husson, O., 2013. Redox potential (eh) and pH as drivers of soil/plant/microorganism systems: a transdisciplinary overview pointing to integrative opportunities for agronomy. Plant and Soil 362, 389–417. https://doi.org/10.1007/s11104-012-1429-7.
IUSS Working Group, 2022. World Reference Base for Soil Resources. International Soil Classification System for Naming Soils and Creating Legends for Soil Maps, fourth ed. International Union of Soil Sciences (IUSS).
Jačka, L., Walmsley, A., Kovář, M., Frouz, J., 2021. Effects of different tree species on infiltration and preferential flow in soils developing at a clayey spoil heap. Geoderma 403, 115372. https://doi.org/10.1016/j.geoderma.2021.115372.
Jänsch, S., Steffens, L., Höfer, H., Horak, F., Roß-Nickoll, M., Russell, D., Toschki, A., Römbke, J., 2013. State of knowledge of earthworm communities in German soils as a basis for biological soil quality assessment. Soil Organisms 85, 215–233.
Jégou, D., Cluzeau, D., Hallaire, V., Balesdent, J., Tréhen, P., 2000. Burrowing activity of the earthworms Lumbricus terrestris and Aporrectodea giardi and consequences on C transfers in soil. European Journal of Soil Biology 36, 27–34. https://doi.org/10.1016/S1164-5563(00)01046-3.
Jordan, D., Li, F., Ponder, F., Berry, E.C., Hubbard, V.C., Kim, K.Y., 1999. The effects of forest practices on earthworm populations and soil microbial biomass in a hardwood forest in Missouri. Applied Soil Ecology 13, 31–38. https://doi.org/10.1016/S0929-1393(99)00017-7.
Joschko, M., Diestel, H., Larink, O., 1989. Assessment of earthworm burrowing efficiency in compacted soil with a combination of morphological and soil physical measurements. Biology and Fertility of Soils 8. https://doi.org/10.1007/BF00266478.
Jost, G., Schume, H., Hager, H., Markart, G., Kohl, B., 2012. A hillslope scale comparison of tree species influence on soil moisture dynamics and runoff processes during intense rainfall. Journal of Hydrology 420–421, 112–124. https://doi.org/10.1016/j.jhydrol.2011.11.057.
Keller, T., Or, D., 2022. Farm vehicles approaching weights of sauropods exceed safe mechanical limits for soil functioning. Proceedings of the National Academy of Sciences of the United States of America 119, e2117699119. https://doi.org/10.1073/pnas.2117699119.
Kinter, E.B., Diamond, S., 1956. A new method for preparation and treatment of oriented-aggregate specimens of soil clays for X-ray diffraction analysis. Soil Science 81, 111–120.
Klein-Raufhake, T., Hölzel, N., Schaper, J.J., Hortmann, A., Elmer, M., Fornfeist, M., Linnemann, B., Meyer, M., Rentemeister, K., Santora, L., Wöllecke, J., Hamer, U., 2024. Severity of topsoil compaction controls the impact of skid trails on soil ecological processes. Journal of Applied Ecology 61, 1817–1828. https://doi.org/10.1111/1365-2664.14708.
Klöffel, T., Jarvis, N., Yoon, S.W., Barron, J., Giménez, D., 2022. Relative entropy as an index of soil structure. European Journal of Soil Science 73, e13254.

Koestel, J., 2018. SoilJ: an ImageJ plugin for the semiautomatic processing of three-dimensional X-Ray images of soils. Vadose Zone Journal 17, 1–7. https://doi.org/10.2136/vzj2017.03.0062.
Koestel, J., Schlüter, S., 2019. Quantification of the structure evolution in a garden soil over the course of two years. Geoderma 338, 597–609. https://doi.org/10.1016/j.geoderma.2018.12.030.
Kooch, Y., Zaccone, C., Lamersdorf, N.P., Tonon, G., 2014. Pit and mound influence on soil features in an Oriental beech (Fagus orientalis lipsky) forest. European Journal of Forest Research 133, 347–354. https://doi.org/10.1007/s10342-013-0766-2.
Kupka, D., Gruba, P., 2022. Effect of pH on the sorption of dissolved organic carbon derived from six tree species in forest soils. Ecological Indicators 140, 108975. https://doi.org/10.1016/j.ecolind.2022.108975.
Le Couteulx, A., Wolf, C., Hallaire, V., Pérès, G., 2015. Burrowing and casting activities of three endogeic earthworm species affected by organic matter location. Pedobiologia 58, 97–103. https://doi.org/10.1016/j.pedobi.2015.04.004.
Legland, D., Arganda-Carreras, I., Andrey, P., 2016. MorphoLibJ: integrated library and plugins for mathematical morphology with ImageJ. Bioinformatics 32, 3532–3534. https://doi.org/10.1093/bioinformatics/btw413.
Lenth, R.V., 2025. Emmeans: estimated marginal means, Aka least-squares means. https://doi.org/10.32614/CRAN.package.emmeans.
Leuther, F., Mikutta, R., Wolff, M., Kaiser, K., Schlüter, S., 2023. Structure turnover times of grassland soils under different moisture regimes. Geoderma 433, 116464. https://doi.org/10.1016/j.geoderma.2023.116464.
Lucas, M., Nguyen, L.T.T., Guber, A., Kravchenko, A.N., 2022. Cover crop influence on pore size distribution and biopore dynamics: enumerating root and soil faunal effects. Frontiers of Plant Science 13, 928569. https://doi.org/10.3389/fpls.2022.928569.
Ma, L., Shao, M., Fan, J., Wang, J., Li, Y., 2021. Effects of earthworm (Metaphire guillelmi) density on soil macropore and soil water content in typical anthrosol soil. Agriculture, Ecosystems & Environment 311, 107338. https://doi.org/10.1016/j.agee.2021.107338.
Matuschek, H., Kliegl, R., Vasishth, S., Baayen, H., Bates, D., 2017. Balancing type I error and power in linear mixed models. Journal of Memory and Language 94, 305–315. https://doi.org/10.1016/j.jml.2017.01.001.
McNabb, D.H., Startsev, A.D., Nguyen, H., 2001. Soil wetness and traffic level effects on bulk density and air-filled porosity of compacted boreal forest soils. Soil Science Society of America Journal 65, 1238–1247. https://doi.org/10.2136/sssaj2001.6541238x.
Mercier, P., Aas, G., Dengler, J., 2019. Effects of skid trails on understory vegetation in forests: a case study from northern Bavaria (germany). Forest Ecology and Management 453, 117579. https://doi.org/10.1016/j.foreco.2019.117579.
Midway, S., Robertson, M., Flinn, S., Kaller, M., 2020. Comparing multiple comparisons: practical guidance for choosing the best multiple comparisons test. PeerJ 8, e10387. https://doi.org/10.7717/peerj.10387.
Moore, D.M., Reynolds, J.R.C., 1989. X-ray Diffraction and the Identification and Analysis of Clay Minerals.
Mossadeghi-Björklund, M., Arvidsson, J., Keller, T., Koestel, J., Lamandé, M., Larsbo, M., Jarvis, N., 2016. Effects of subsoil compaction on hydraulic properties and preferential flow in a Swedish clay soil. Soil and Tillage Research 156, 91–98. https://doi.org/10.1016/j.still.2015.09.013.
Muys, B., 1989. Evaluation of Conversion of Tree Species and Liming as Measures to Decrease Soil Compaction in a Beech Forest on Loamy Soil. https://doi.org/10.21825/sg.v54i0.907. SG 54.
Nakagawa, S., 2004. A farewell to bonferroni: the problems of low statistical power and publication bias. Behavioral Ecology 15, 1044–1045. https://doi.org/10.1093/beheco/arh107.
Naylor, D., McClure, R., Jansson, J., 2022. Trends in microbial community composition and function by soil depth. Microorganisms 10, 540. https://doi.org/10.3390/microorganisms10030540.
Nazari, M., Arthur, E., Lamandé, M., Keller, T., Bilyera, N., Bickel, S., 2023. A meta-analysis of soil susceptibility to machinery-induced compaction in forest ecosystems across global climatic zones. Curr. For. Rep. 9, 370–381. https://doi.org/10.1007/s40725-023-00197-y.
Nazari, M., Eteghadipour, M., Zarebanadkouki, M., Ghorbani, M., Dippold, M.A., Bilyera, N., Zamanian, K., 2021. Impacts of logging-associated compaction on forest soils: a meta-analysis. Front. For. Glob. Change 4, 780074. https://doi.org/10.3389/ffgc.2021.780074.
Page-Dumroese, D.S., Jurgensen, M.F., Tiarks, A.E., Ponder, Jr. F., Sanchez, F.G., Fleming, R.L., Kranabetter, J.M., Powers, R.F., Stone, D.M., Elioff, J.D., Scott, D.A., 2006. Soil physical property changes at the north American long-term soil productivity study sites: 1 and 5 years after compaction. Can. J. For. Res. 36, 551–564. https://doi.org/10.1139/x05-273.
Peth, S., Nellesen, J., Fischer, G., Horn, R., 2010. Non-invasive 3D analysis of local soil deformation under mechanical and hydraulic stresses by μCT and digital image correlation. Soil and Tillage Research 111, 3–18. https://doi.org/10.1016/j.still.2010.02.007.
Phillips, H.R.P., Guerra, C.A., Bartz, M.L.C., Briones, M.J.I., Brown, G., Crowther, T.W., Ferlian, O., Gongalsky, K.B., Van Den Hoogen, J., Krebs, J., Orgiazzi, A., Routh, D., Schwarz, B., Bach, E.M., Bennett, J.M., Brose, U., Decaëns, T., König-Ries, B., Loreau, M., Mathieu, J., Mulder, C., Van Der Putten, W.H., Ramirez, K.S., Rillig, M. C., Russell, D., Rutgers, M., Thakur, M.P., De Vries, F.T., Wall, D.H., Wardle, D.A., Arai, M., Ayuke, F.O., Baker, G.H., Beauséjour, R., Bedano, J.C., Birkhofer, K., Blanchart, E., Blossey, B., Bolger, T., Bradley, R.L., Callaham, M.A., Capowiez, Y., Caulfield, M.E., Choi, A., Crotty, F.V., Crumsey, J.M., Dávalos, A., Diaz Cosin, D.J., Dominguez, A., Duhour, A.E., Van Eekeren, N., Emmerling, C., Falco, L.B., Fernández, R., Fonte, S.J., Fragoso, C., Franco, A.L.C., Fugère, M., Fusilero, A.T., Gholami, S., Gundale, M.J., López, M.G., Hackenberger, D.K., Hernández, L.M., Hishi, T., Holdsworth, A.R., Holmstrup, M., Hopfensperger, K.N., Lwanga, E.H., Huhta, V., Hurisso, T.T., Iannone, B.V., Iordache, M., Joschko, M., Kaneko, N., Kanianska, R., Keith, A.M., Kelly, C.A., Kernecker, M.L., Klaminder, J., Koné, A.W., Kooch, Y., Kukkonen, S.T., Lalthanzara, H., Lammel, D.R., Lebedev, I.M., Li, Y., Jesus Lidon, J.B., Lincoln, N.K., Loss, S.R., Marichal, R., Matula, R., Moos, J.H., Moreno, G., Morón-Ríos, A., Muys, B., Neirynck, J., Norgrove, L., Novo, M., Nuutinen, V., Nuzzo, V., Mujeeb, Rahman P., Pansu, J., Paudel, S., Pérès, G., Pérez-Camacho, L., Piñeiro, R., Ponge, J.-F., Rashid, M.I., Rebollo, S., Rodeiro-Iglesias, J., Rodríguez, M.Á., Roth, A.M., Rousseau, G.X., Rozen, A., Sayad, E., Van Schaik, L., Scharenbroch, B.C., Schirrmann, M., Schmidt, O., Schröder, B., Seeber, J., Shashkov, M.P., Singh, J., Smith, S.M., Steinwandter, M., Talavera, J.A., Trigo, D., Tsukamoto, J., De Valença, A.W., Vanek, S.J., Virto, I., Wackett, A.A., Warren, M.W., Wehr, N.H., Whalen, J.K., Wironen, M.B., Wolters, V., Zenkova, I.V., Zhang, W., Cameron, E.K., Eisenhauer, N., 2019. Global distribution of earthworm diversity. Science 366, 480–485. https://doi.org/10.1126/science.aax4851.
Picchio, R., Mederski, P.S., Tavankar, F., 2020. How and how much, do harvesting activities affect forest soil, regeneration and stands? Current Forestry Reports 6, 115–128.
Pinheiro, J., Bates, D., R Core Team, 2025. Nlme: Linear and nonlinear mixed effects models. https://doi.org/10.32614/CRAN.package.nlme.
Pinheiro, J.C., Bates, D.M., 2000. Mixed-Effects Models in S and S-PLUS. Springer, New York. https://doi.org/10.1007/b98882.
Pöhlitz, J., Rücknagel, J., Schlüter, S., Vogel, H.-J., Christen, O., 2019. Computed tomography as an extension of classical methods in the analysis of soil compaction, exemplified on samples from two tillage treatments and at two moisture tensions. Geoderma 346, 52–62. https://doi.org/10.1016/j.geoderma.2019.03.023.
R Core Team, 2025. R: a Language and Environment for Statistical Computing. R Foundation for Statistical Computing, Vienna, Austria.
Rabot, E., Wiesmeier, M., Schlüter, S., Vogel, H.-J., 2018. Soil structure as an indicator of soil functions: a review. Geoderma 314, 122–137. https://doi.org/10.1016/j.geoderma.2017.11.009.
Renard, P., Allard, D., 2013. Connectivity metrics for subsurface flow and transport. Advances in Water Resources 51, 168–196. https://doi.org/10.1016/j.advwatres.2011.12.001.
Riggert, R., Fleige, H., Horn, R., 2019. An assessment scheme for soil degradation caused by forestry machinery on skid trails in Germany. Soil Science Society of America Journal 83. https://doi.org/10.2136/sssaj2018.07.0255.
Rundgren, S., 1975. Vertical distribution of lumbricids in southern Sweden. Oikos 26, 299. https://doi.org/10.2307/3543500.
Schaefer, M., 1992. Brohmer - fauna von Deutschland: ein Bestimmungsbuch unserer heimischen Tierwelt, 18., neu bearbeitete und neu gestaltete Auflage. In: Bestimmungsbücher, Meyer (Ed.), Quelle Und Meyer Verlag. Heidelberg Wiesbaden.
Schäffer, J., 2022. Recovery of soil structure and fine root distribution in compacted forest soils. Soil Systems 6, 49. https://doi.org/10.3390/soilsystems6020049.
Schelfhout, S., Mertens, J., Verheyen, K., Vesterdal, L., Baeten, L., Muys, B., De Schrijver, A., 2017. Tree species identity shapes earthworm communities. Forests 8, 85. https://doi.org/10.3390/f8030085.
Schindelin, J., Arganda-Carreras, I., Frise, E., Kaynig, V., Longair, M., Pietzsch, T., Preibisch, S., Rueden, C., Saalfeld, S., Schmid, B., Tinevez, J.-Y., White, D.J., Hartenstein, V., Eliceiri, K., Tomancak, P., Cardona, A., 2012. Fiji: an open-source platform for biological-image analysis. Nature Methods 9, 676–682. https://doi.org/10.1038/nmeth.2019.
Schlüter, S., Leuther, F., Albrecht, L., Hoeschen, C., Kilian, R., Surey, R., Mikutta, R., Kaiser, K., Mueller, C.W., Vogel, H.-J., 2022. Microscale carbon distribution around pores and particulate organic matter varies with soil moisture regime. Nature Communications 13, 2098. https://doi.org/10.1038/s41467-022-29605-w.
Schlüter, S., Sheppard, A., Brown, K., Wildenschild, D., 2014. Image processing of multiphase images obtained via x-ray microtomography: a review. Water Resources Research 50, 3615–3639. https://doi.org/10.1002/2014WR015256.
Shah, A.N., Tanveer, M., Shahzad, B., Yang, G., Fahad, S., Ali, S., Bukhari, M.A., Tung, S. A., Hafeez, A., Souliyanonh, B., 2017. Soil compaction effects on soil health and cropproductivity: an overview. Environmental Science & Pollution Research 24, 10056–10067. https://doi.org/10.1007/s11356-017-8421-y.
Shestak, C.J., Busse, M.D., 2005. Compaction alters physical but not biological indices of soil health. Soil Science Society of America Journal 69, 236. https://doi.org/10.2136/sssaj2005.0236.
Sims, R.W., Gerard, B.M., 1985. Earthworms: Keys and Notes for the Identification and Study of the Species. Brill, Archive.
Sohrabi, H., Jourgholami, M., Jafari, M., Shabanian, N., Venanzi, R., Tavankar, F., Picchio, R., 2020a. Soil recovery assessment after timber harvesting based on the sustainable forest operation (SFO) perspective in Iranian temperate forests. Sustainability 12, 2874. https://doi.org/10.3390/su12072874.
Sohrabi, H., Jourgholami, M., Jafari, M., Tavankar, F., Venanzi, R., Picchio, R., 2020b. Earthworms as an ecological indicator of soil recovery after mechanized logging operations in mixed beech forests. Forests 12, 18. https://doi.org/10.3390/f12010018.
Sohrabi, H., Jourgholami, M., Lo Monaco, A., Picchio, R., 2022. Effects of forest harvesting operations on the recovery of earthworms and nematodes in the hyrcanain old-growth forest: assessment, mitigation, and best management practice. Land 11, 746. https://doi.org/10.3390/land11050746.
Startsev, A.D., McNabb, D.H., 2009. Effects of compaction on aeration and morphology of boreal forest soils in Alberta, Canada. Canadian Journal of Soil Science 89, 45–56. https://doi.org/10.4141/CJSS06037.
Tavankar, F., Nikooy, M., Ezzati, S., Jourgholami, M., Latterini, F., Venanzi, R., Picchio, R., 2022. Long-term assessment of soil physicochemical properties and

seedlings establishment after skidding operations in mountainous mixed hardwoods. European Journal of Forest Research 141, 571–585. https://doi.org/10.1007/s10342-022-01461-9.

Teepe, R., Brumme, R., Beese, F., Ludwig, B., 2004. Nitrous oxide emission and methane consumption following compaction of forest soils. Soil Science Society of America Journal 68, 605–611. https://doi.org/10.2136/sssaj2004.6050.

Thorez, J., 1975. Phyllosilicates and clay minerals: a laboratory handbook for their x-ray diffraction analysis. Editions G. Lelotte, Liège, pp. 1–579.

Tributh, H., 1991. Notwendigkeit und Vorteil der Aufbereitung von Boden- und Lagerstättentonen. In: Tributh, H., Lagaly, G. (Eds.), Identifizierung Und Charakterisierung Von Tonmineralen, Berichte Der DTTG, pp. 29–33. Giessen.

Valckx, J., Govers, G., Hermy, M., Muys, B., 2011. Optimizing earthworm sampling in ecosystems. In: Karaca, A. (Ed.), Biology of Earthworms. Springer Berlin Heidelberg, Berlin, Heidelberg, pp. 19–38. https://doi.org/10.1007/978-3-642-14636-7_2.

Von Wilpert, K., Schäffer, J., 2006. Ecological effects of soil compaction and initial recovery dynamics: a preliminary study. European Journal of Forest Research 125, 129–138. https://doi.org/10.1007/s10342-005-0108-0.

Wallace, B., Bulmer, C., Hope, G., Curran, M., Philpott, T., Murray, M., 2021. Soil compaction and organic matter removal effects on soil properties and tree growth in the interior Douglas-fir zone of southern British Columbia. Forest Ecology and Management 494, 119268. https://doi.org/10.1016/j.foreco.2021.119268.

Whittig, L.D., 1965. X-ray diffraction techniques for mineral identification and mineralogical composition. In: Black, C.A. (Ed.), Methods of Soil Analysis. American Society of Agronomy, Madison, Wisconsin, pp. 671–698.

Wilson, M.J., 1987. A Handbook of Determinative Methods in Clay Mineralogy. Blackie, Glasgow and London.

Wu, D., Du, E., Eisenhauer, N., Mathieu, J., Chu, C., 2025. Global engineering effects of soil invertebrates on ecosystem functions. Nature 640, 120–129. https://doi.org/10.1038/s41586-025-08594-y.

Zanella, A., Katzensteiner, K., Ponge, J.-F., Jabiol, B., Sartori, G., Kolb, E., Le Bayon, R.-C., Aubert, M., Ascher-Jenull, J., Englisch, M., Hager, H., 2019. *TerrHum*: an iOS application for classifying terrestrial humipedons and some considerations about soil classification. Soil Science Society of America Journal 83. https://doi.org/10.2136/sssaj2018.07.0279.

Zicsi, A., Szlavecz, K., Csuzdi, C., 2011. Leaf litter acceptance and cast deposition by peregrine and endemic European lumbricids (oligochaeta: lumbricidae). Pedobiologia 54, S145–S152. https://doi.org/10.1016/j.pedobi.2011.09.004.